Technical Report Documentation Page

| 1. Report No. | 2. Government Accession No. | 3. Recipient's Catalog No. |
|---|---|---|
| | | |

4. Title and Subtitle
**The Feasibility of Using Electro-Rheological Fluids in Aircraft Flight Controls**

5. Report Date
**March 1990**

6. Performing Organization Code

7. Author(s)
**Zheng Lou, Robert D. Ervin, Frank E. Filisko**

8. Performing Organization Report No.
**UMTRI-90-10**

9. Performing Organization Name and Address
The University of Michigan
Transportation Research Institute
2901 Baxter Road, Ann Arbor, Michigan 48109

10. Work Unit No. (TRAIS)

11. Contract or Grant No.
**P.O. 1122**

12. Sponsoring Agency Name and Address
**Dynamic Controls, Inc.**
7060 Cliffwood Place
Dayton, OH 45424

13. Type of Report and Period Covered
**Final: 5/22/89 - 1/30/90**

14. Sponsoring Agency Code

15. Supplementary Notes

16. Abstract

A "Phase-1" study was conducted to develop experimental data and general analyses needed for the determination of the feasibility of using electro-rheological (ER) fluids in hydraulic devices for controlling the motions of aircraft in flight. Such fluids constitute specially-formulated materials which exhibit large changes in their viscosity in response to an intense electrical field, thereby enabling electrical control of mechanical responses.

An ER devices laboratory is described and experimental results presented. ER valves designed for basic study of flow control are presented. Three ER fluid specimens were formulated and subjected to a matrix of measurements showing qualities of wide bandwidth (at least 1 kHz), high thermal stability at temperatures up to 125 or 150 degrees C, and moderate shear stress limits (approximately 0.1 psi). The performances of a single ER valve and a four-arm bridge using multiple valves have been analyzed, showing that a functional and efficient ER bridge is feasible.

The results suggest that it is feasible to build an ER-controlled first-stage bridge circuit for modulating the flow to a power spool which would, thence, control flow to a flight-control actuator. A parallel-plate design concept for the ER valves to be used in this bridge is described, and a prototype was constructed. Assuming a fluid yield stress limit of 0.1 psi and an active valve length of 1.5 meters, each valve will deliver up to 300 psi pressure drop as required in the first-stage device.

| 17. Key Words | 18. Distribution Statement |
|---|---|
| **Electro-rheological fluids, field-dependent fluids, water-free fluids, servo-control, valves, hydraulics** | |

| 19. Security Classif. (of this report) | 20. Security Classif. (of this page) | 21. No. of Pages | 22. Price |
|---|---|---|---|
| | | **73** | |

# TABLE OF CONTENTS

# 1. INTRODUCTION

This report presents the results of a study entitled "The Feasibility of Using Field-Dependent Fluids in Flight Controls." The work was sponsored by the U.S. Air Force and conducted by the University of Michigan Transportation Research Institute and the Department of Materials Science and Engineering of the College of Engineering under subcontract from Dynamic Controls, Inc. The study examines so-called electro-rheological, or field-dependent, fluids as the working medium upon which electrohydraulic control systems may be designed for aircraft flight controls. Such fluids constitute specially-formulated materials which exhibit large changes in their viscosity in response to an intense electrical field. Devices employing such fluids typically involve a working section where the fluid flows between two parallel plates upon which a high voltage is imposed. The increased viscosity of the fluid in response to the electrical field causes a pressure drop that, in turn, yields some desired mechanical response. While many other embodiments are possible, in every case a high intensity electrical field alters the fluid's stress response to strain.

This study has involved both analytical and experimental efforts intended to illustrate the feasibility of using such fluids in the flight control application. In Chapter 2 of this report, an experimental apparatus designed for examination of fluid response properties is described. The apparatus was employed in the ER Devices Laboratory at the University of Michigan Transportation Research Institute (UMTRI.) The objective of the Laboratory is to develop device and systems technology permitting application of ER fluids. The scope of effort covers characterization of the properties of ER fluids, testing ER valve design concepts, measuring the flow characteristics of ER valves and bridges, and testing the compatibility between ER fluids and conventional fluid power systems.

Chapter 3 presents the design of two prototype ER valves which were fabricated in the lab. The valves provide for direct characterization of pressure/flow relationships, both in a simple device having a very short working section and a labyrinth device having a much longer working section for achieving high net pressure drops.

A set of measurements was completed during this study using a device that is commonly known as a "rheometer", or "viscometer". The measurements were conducted in the UMTRI lab for each of a group of fluid samples that had been formulated and prepared within the University's Department of Materials Science and Engineering. The fluids employ materials which contain no significant fraction of water molecules and, thus, are quite distinct from ER fluids which have been the object of study since the late 1940s. The test results are presented and analyzed in Chapter 4 of this report.

The experimental results address basic properties including the dynamic bandwidth, the temperature sensitivity, the current density response of the ER fluids, and the influence of fractional content of solid materials. No attempt has been made here to explain the mechanisms of

ER fluids, although the data from this study may have inferential value in this respect. Methodological problems encountered in the characterization of ER fluids are also discussed in chapter 4. One of these issues involves the problem of characterizing a fluid having a bandwidth of 1 kHz or higher with an apparatus having many mechanical resonances at frequencies throughout the 0-to-1kHz band. Another methodological problem involves identification of the electrical current which is carried conductively through the ER fluid.

Chapter 5 presents two analyses of the basic characteristics of ER valves and bridges. The analyses form the basis for projecting the performance qualities of a cluster of four ER valves employed in a bridge-type hydraulic circuit.

Finally, in Chapter 6, main conclusions from this study are listed. It is recommended that, in the next phase of the project, a four-valve ER bridge be constructed as the pilot stage of an electrohydraulic control valve.

# 2. ER FLUIDS LABORATORY

The ER Fluids Laboratory at UMTRI was equipped, during this project, with an ER fluid viscometer and an ER fluid valve apparatus. A third apparatus involving a simple hydraulic circuit for examination of long term durability issues during steady operation, was designed for later assembly. The viscometer and valve apparatuses will be described in this section.

## 2.1. An ER Fluid Viscometer

The purpose of a fluid viscometer is to enable study of the rheology of ER fluids, with particular interest in characterizing the fluid properties which will govern the design of ER valve, bridge, and system packages.

Cup: (a container which holds the ER fluid sample and forms the outer surface of a shear annulus.)

Bob: (a rotated cylinder, immersed in the cup, which forms the inner surface of the shear annulus.)

ER fluid: (the test sample.)

Torque transducer: (providing the mounting base for the Cup, thereby permitting measurement of a mechanical response which reflects the shear behavior of the ER fluid sample.)

D.C. motor and control: (driving the Bob and providing rotational speed control.)

High-voltage amplifier: (amplifying the output of a precision signal generator from a few volts to the kilovolt range required between the Bob and the Cup.)

Power supply: (providing power to the high-voltage amplifier.)

Macintosh II: (a microcomputer employed in the overall operation of the viscometer. The computer controls a wave generator, a high-voltage amplifier and a motor controller. It also collects and processes the transduced torque signal.)

Optical isolator: (providing protection to the microcomputer against extraneous voltage transients coming back through its signal output lines.)

Roto-pulser: (providing feed-back signal to the motor controller and serving to transduce the rate of rotational shear between the Cup and the Bob.)

Signal conditioner: (a system for digital sampling and scaling from analog data.)

Wave generator: (generating signals of different wave forms and frequencies for excitation of the ER device.)

In addition, a temperature control system, not shown in Fig. 2.1, was employed for achieving a desired fluid temperature during the experiment. The controller consists of a thermocouple, a thermocouple read-out meter, a heating mat and a voltage regulator. In the experiments reported here, the temperature was controlled through manual adjustment of a voltage regulator. Subsequent measurements will be conducted using an automatic temperature controller which has been purchased.

The measurements made using the described viscometer are presented in Chapter 4.

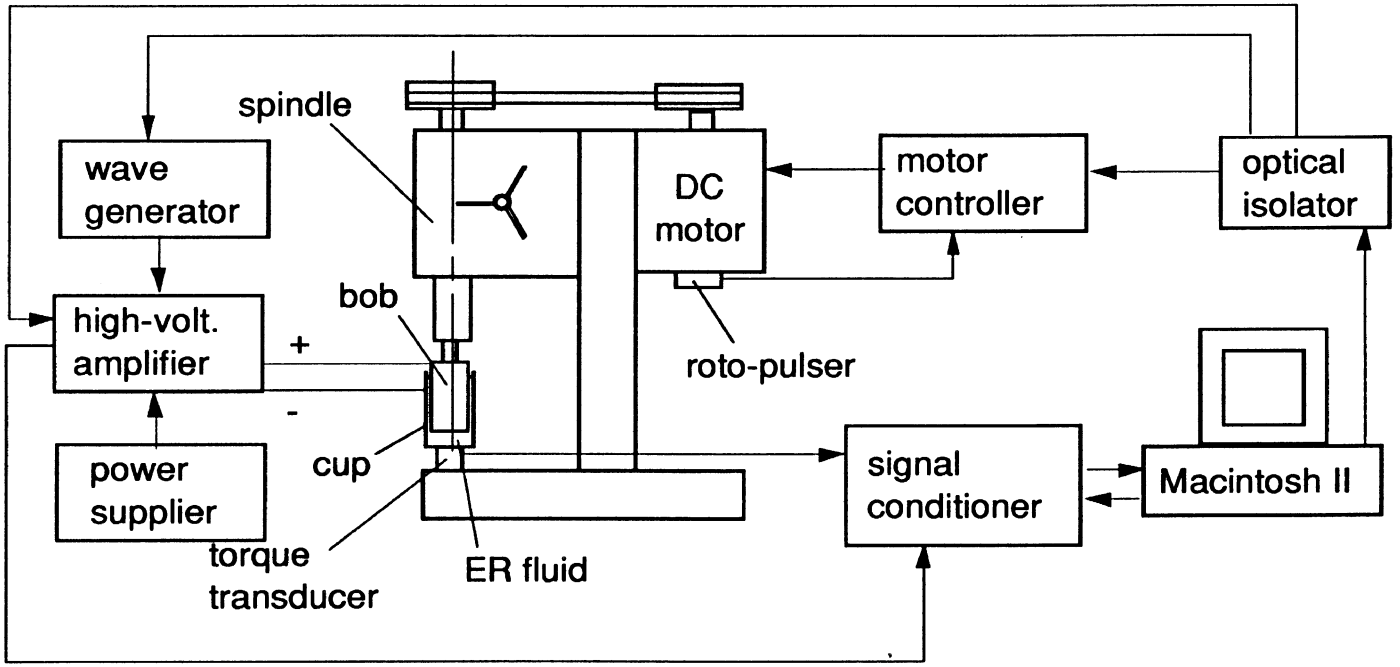


Fig. 2.1 ER Fluid Viscometer.

## 2.2. An ER Fluid Valve Tester

A second device constructed for this study involved a hydraulic circuit for delivering a small volume of ER fluid in a rather steady flow condition to either of two constructed valves. The apparatus provides for measurement of both the pressure drop and total flow condition at each valve, using a circuit whose design was driven primarily by the need to make measurements using small volumes of fluid, since no commercial source of such fluids currently exists for obtaining bulk samples. The apparatus was intended to provide for the study of the following:

(1) the Bingham stress exhibited by the ER fluid sample (that is, the static stress which the fluid exhibits in its "solid" condition, under influence of a strong electric field.)

(2) the rheology of the ER fluids under steady flow, especially with high frequency variation in the imposed electrical field.)

(3) the pressure-flow relationship for different ER valve designs.

(4) the pressure-flow relationship achieved across the diagonal of a 4-arm ER bridge (a hydraulic analog to the electrical circuit of a wheatstone bridge; to be discussed in detail in Chapter 5.)

The valve-measurement apparatus is illustrated in Figure 2.2 using a part-numbering scheme as defined below:

Part 1. LVDT, Linearly-Variable Differential Transformer: (measures the fluid flow rate by transducing the displacement of a fluid-dispensing cylinder.)

Part 2a. Cylinder (a): (dispenses a limited quantity of ER fluid though the test valves or bridges.)

Part 2b. Cylinder (b): (dispenses/receives the fluid volume and enables measurement of flow rate through displacement of its piston.)

Part 3. Pressure transducers: (measuring the pressure drop across the valve.)

Part 4. Solenoid valve: (providing for circuit control so that data collection can be timed with the brief duration of flow through the valve.)

Part 5. Ball valve: (for charging the system with the ER fluid sample and for bleeding air bubbles.)

Part 6. ER valve: (the test object.)

part 7. Ball valves: (for blocking nitrogen in the tank (part 8) while charging and reloading ER fluids.)

Part 8. Nitrogen tank: (a large volume from which the charge pressure is attained in the ER fluid circuit.)

Part 9. Safety valve: (for protecting the tank and other devices.)

Part 10. Flow rate control valves: (for throttling flow.)

Part 11. Pressure gauge: (indicating nitrogen tank pressure.)

Part 12. Solenoid valve: ( for controlling tank pressure.)

Part 13. Solenoid valve: (for controlling tank pressure.)

Part 14. Cylinder regulator: (for stepping down nitrogen pressure available to the ER charging system.)

Part 15. Nitrogen cylinder: (source of pressurized nitrogen.)

Part 16. Check valve: (preventing air from entering the nitrogen circuit.)

Part 17. 4-way solenoid valve with two solenoids: (for switching the flow direction between cylinders (a) and (b).)

In addition to the parts listed above and shown in Fig.2.2, the valve apparatus employed the same signal generator, amplifier, computer controller, and data collection instruments as cited above relative to the viscometer device.

*Preliminary Test Results*

In the operation of the valve test apparatus, an initial problem arose which prevented the collection of data during the Phase 1 effort. Although the device worked well with pure kerosene (the base fluid for ER samples prepared in this project) operation with actual ER fluids quickly resulted in the ingestion of bubbles into the fluid side of the circuit. It is assumed that the bubbles constitute nitrogen which is leaking around the seals on the two dispensing cylinders, perhaps as a result of seal failure in the presence of the particulate phase of the fluid formula.

*Future Modifications*

To overcome the problem encountered in the preliminary test, the tester will be modified as shown in Fig. 2.3. The function of Part 2a in the original tester will be replaced by Part 18a in the new system while that of Part 2b will be replaced by Parts 18b and 2. Parts 18a and 18b are bladder-type accumulators which will completely seal off the ER circuit. A new cylinder, Part 2, will be used as a nitrogen-to-conventional hydraulic fluid interface, affording precision measurement of fluid flow by means of monitoring the piston displacement.

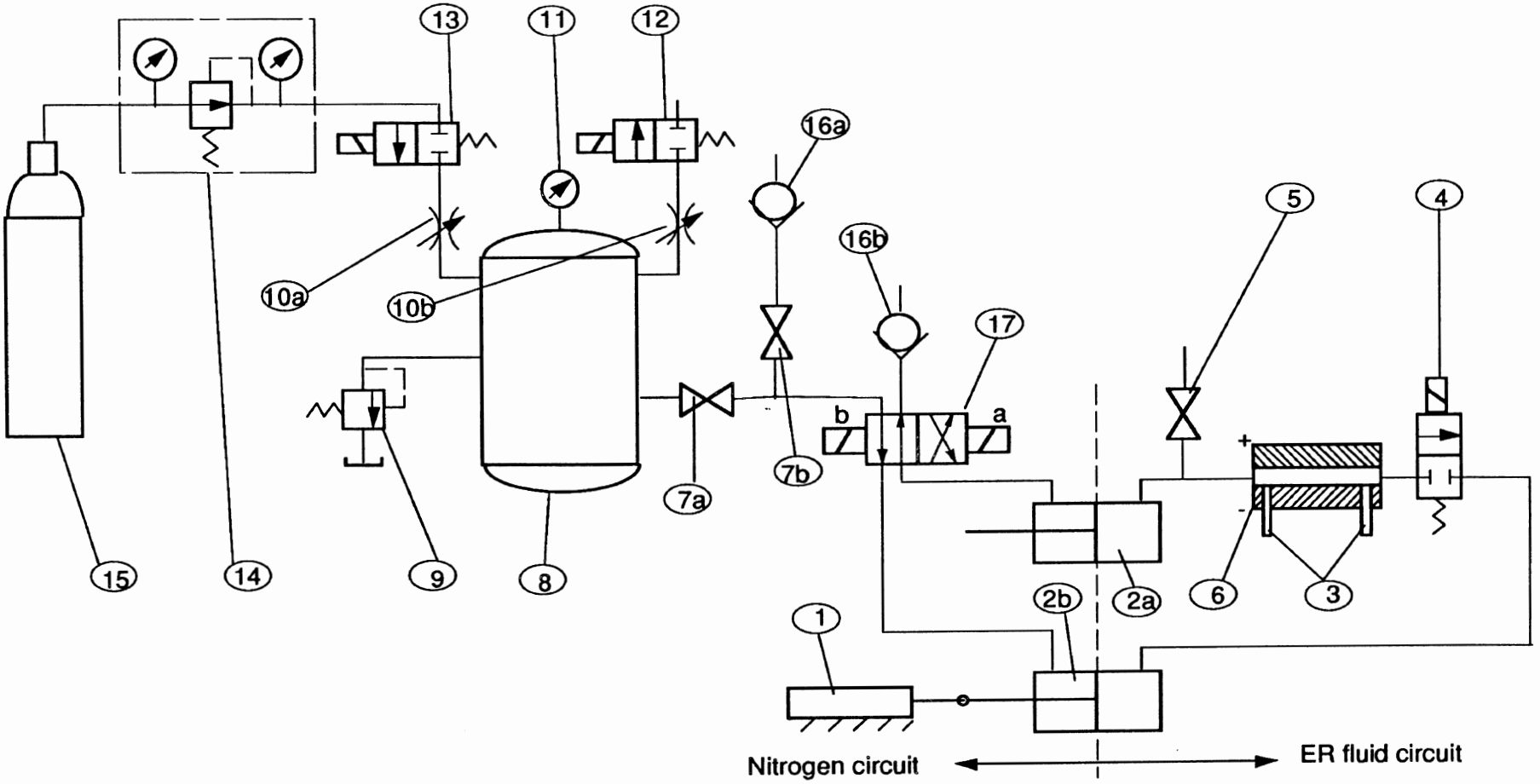


Fig. 2 .2 Original ER Valve Tester .

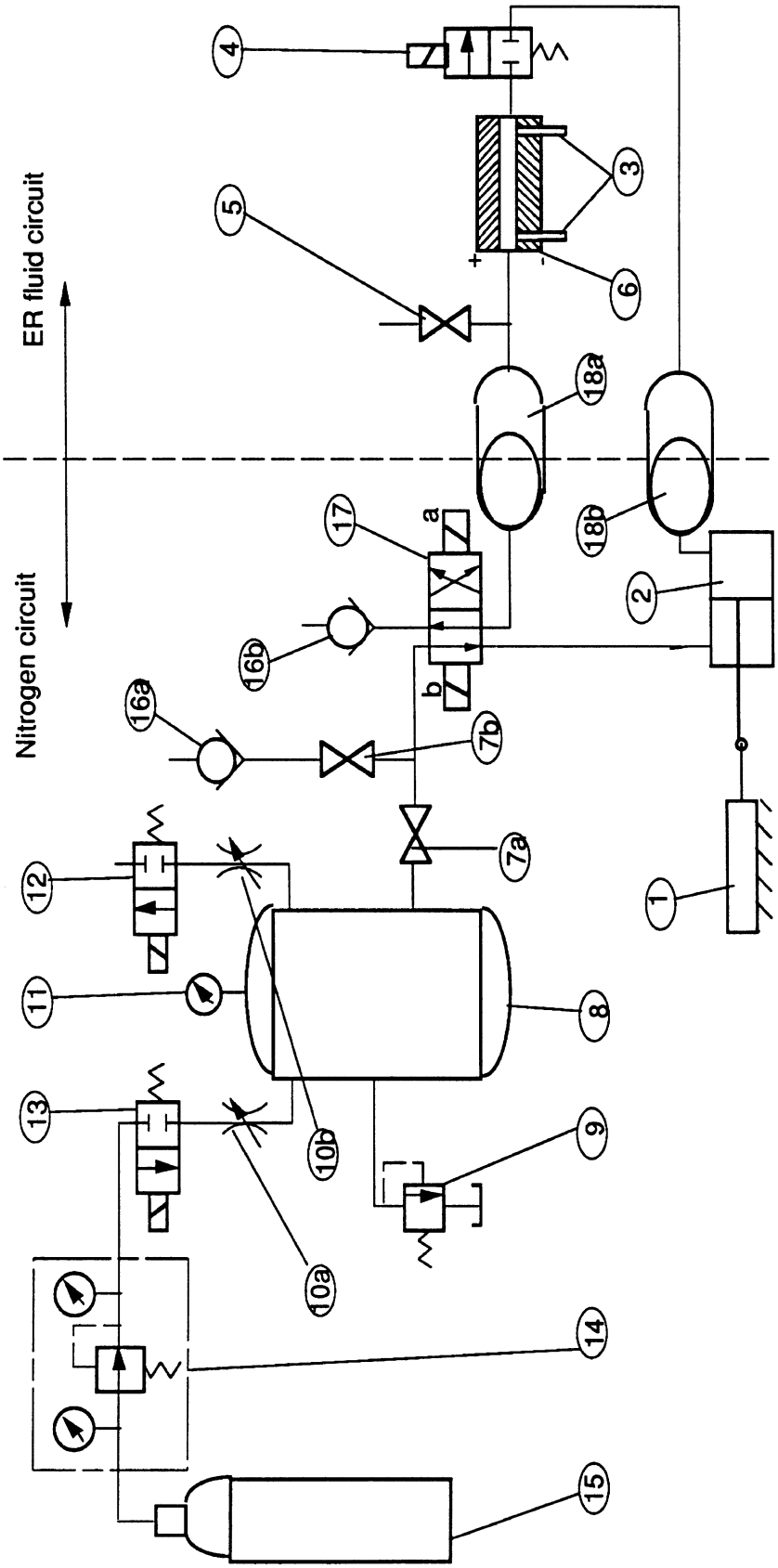


Fig. 2.3 New ER Valve Tester.

## 2.3. An ER Fluid System Tester

*Objectives*

An ER fluid system mockup has been designed as shown in Fig. 2.4. The circuit is intended for use in continuous operation of an ER valve, bridge or actuator system. The system tester has more control over flow rate than pressure—the opposite to the intended approach in the valve test apparatus.

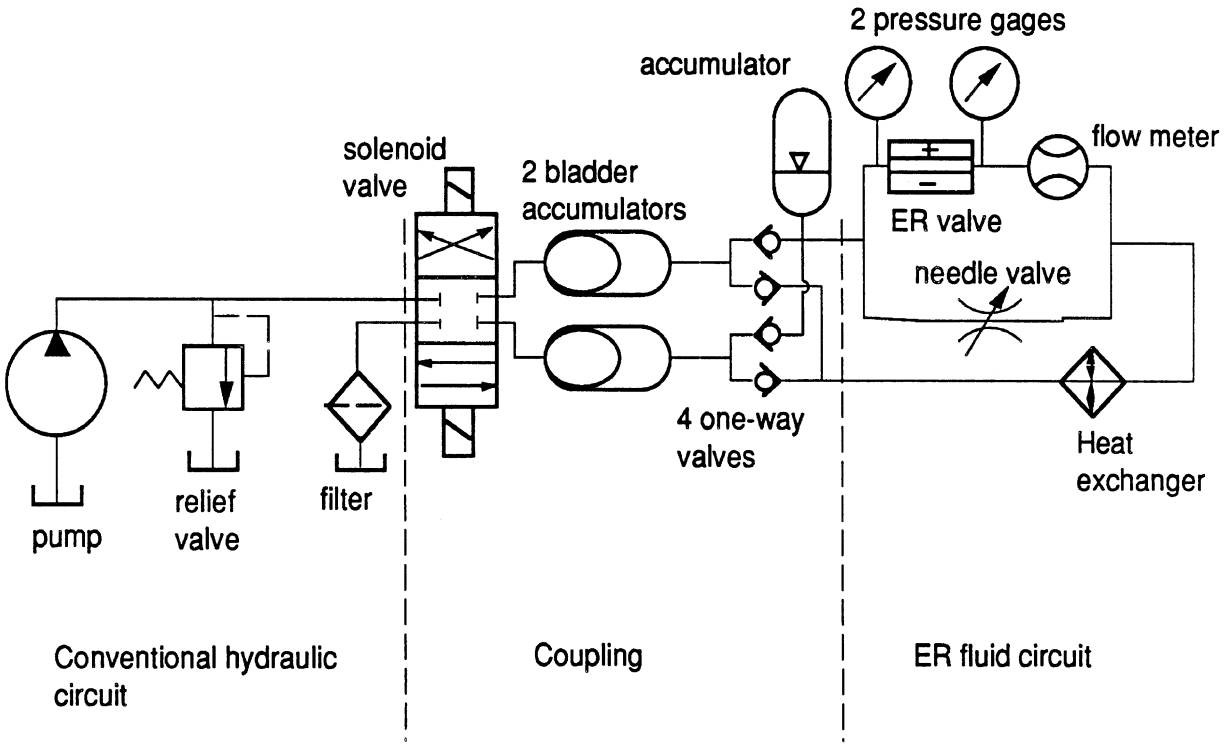


**Fig. 2.4 An ER fluid system tester.**

*Structure (Fig. 2.4)*

The system tester has three sub-circuits: a conventional hydraulic circuit, a coupling, and an ER fluid circuit. The conventional hydraulic circuit provides a continuous power supply. Its working fluid is some conventional hydraulic oil. The ER fluid circuit is the testing section where ER fluids are used. The coupling is used both to transmit power from the conventional hydraulic circuit to the ER fluid circuit and to completely separate two different working fluids. A possible commercial unit is being sought to provide the coupling element, and possibly the conventional hydraulic circuit as well. The functions of individual components in the system tester are listed below:

Accumulator: (to smooth out the pressure fluctuation; to absorb shock.)

Bladder accumulators: (to seal ER fluids from any contaminations; to protect the conventional hydraulic circuit from being invaded by particulates in ER fluids.)

ER valve: (an ER valve, bridge or other package.)

Filter: (for conventional filtration.)

Flow meter: (for measuring the (steady state) flow rate.)

Heat exchanger: (controlling the ER fluid temperature. No heat exchanger is used in the conventional hydraulic circuit where there are no substantial heat-generating frictional losses.)

Needle valve: (bypassing a certain amount of the flow in order to control the flow rate through the ER valve.)

One-way valves: (controlling the flow directions.)

Motor-driven Pump (an external gear type): (supplying the flow.)

Pressure gages : (for monitoring system pressure.)

Relief valve: (for system pressure control.)

Solenoid valve: (for electrical control of the flow directions.)

Tank: (providing the fluid source for the pump and the fluid sink for return flow.)

# 3. VALVE DESIGNS

Two types of ER valves, cylindrical and parallel, have been designed and fabricated in this study. Their tests with kerosene are very normal although they have not been tested yet with the ER fluids due to a problem with the valve tester (Section 2.2).

## 3.1. A Cylindrical Valve

A cylindrical valve has been designed and fabricated as shown in Fig. 3.1. The flow path is formed by the annulus between the valve body (the grounded electrode) and the valve shaft (the positive electrode). The annulus has a gap of 1 mm, a diameter of 12 mm and a length of 20 mm, which offers minimal resistance for an un-energized ER fluid flow. If an ER fluid is energized to have a Bingham stress of 1 psi, the total pressure drop along the annulus will be about 40 psi. If the Bingham stress is 0.1 psi, the pressure drop will be about 4 psi. The valve is not designed to have an industrial application. It is mainly to be used for some basic assessment of the design concept.

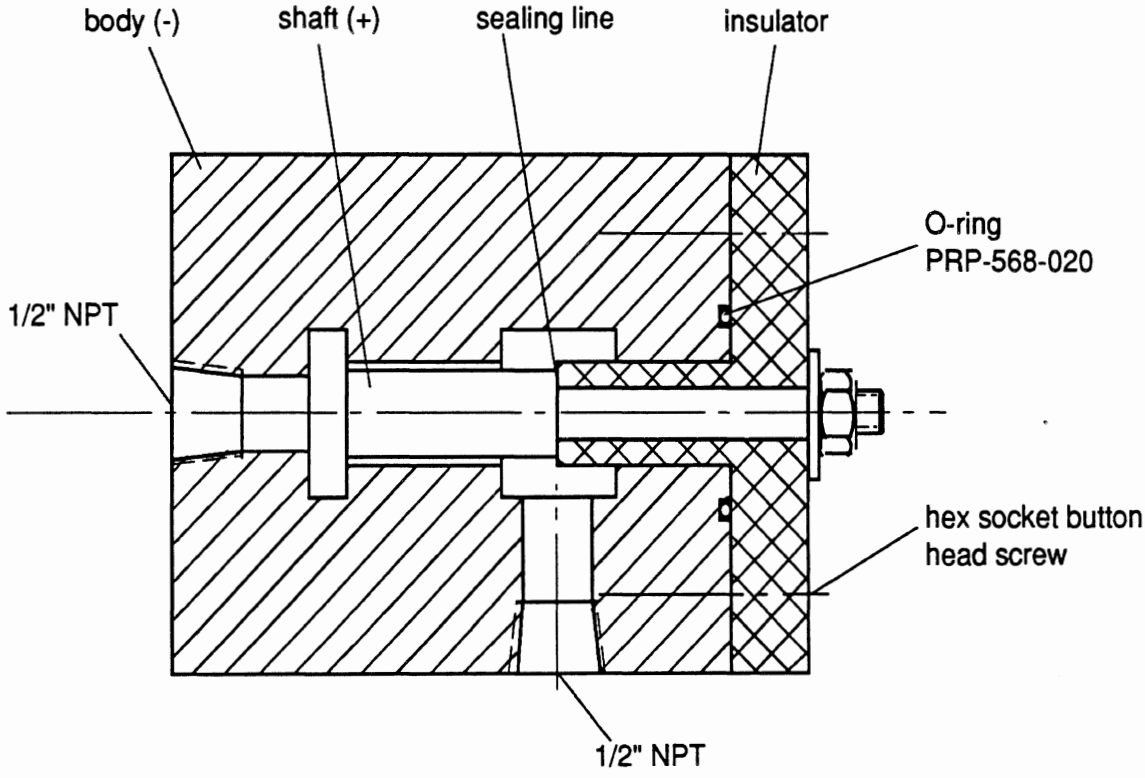


**Fig. 3.1 A cylindrical valve.**

## 3.2. A Parallel-plate Valve

A parallel-plate valve has been designed and fabricated as shown in Fig. 3.2. There are 11 stainless steel plates, 5 of which act as positive electrodes and 6 of which act as ground electrodes. Between every two neighboring electrodes, which are always of opposite polarities, there is a Nylon gallery plate in which a slot (114.3 mm long and 10 mm wide) is cut out. The flow passes through the hole in each stainless steel plate, flows along the slot in the next gallery, and then drops through the next hole into the next gallery—thus alternating directions through the valve stack while accumulating a substantial total length of the shear path through the valve. The total passage length is 1.143 meters through 10 gallery plates. If an ER fluid is energized to have a Bingham stress of 1 psi, the total pressure drop across the valve will be 2,286 psi, which is suitable for the direct control of many high-pressure actuators. If the Bingham stress is 0.1 psi, the pressure drop through the gallery valve will be about 228 psi, which is still enough to drive the main stage spool in a servo valve.

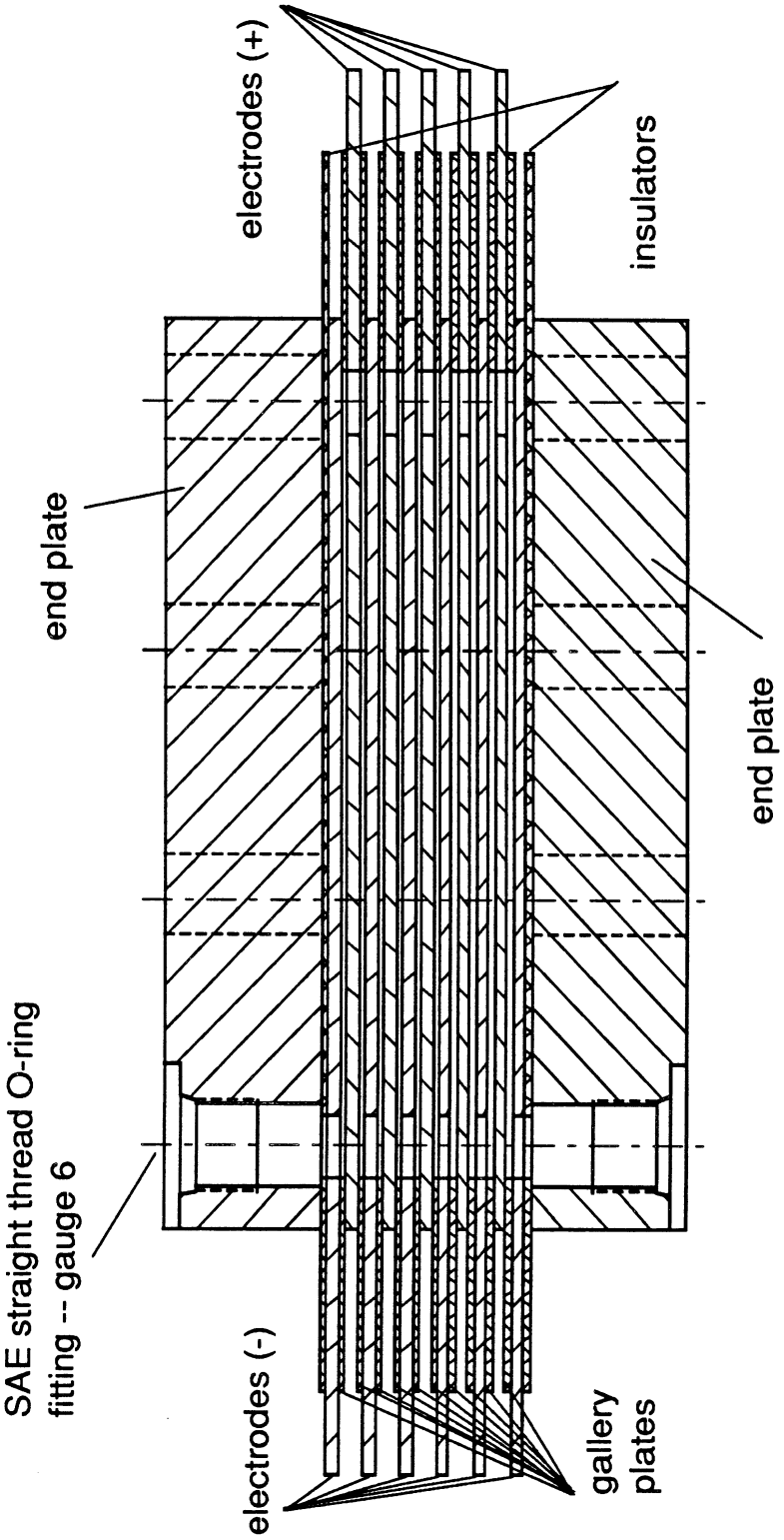


Fig. 3.2. A parallel-plate valve.

# 4. ER FLUIDS CHARACTERIZATION

## 4.1. Fluid compositions and solid contents

Three ER fluids were prepared for this study in the Materials Sciences laboratory of the University of Michigan. Each fluid was identified by a string of characters listed in Table 4.1. In each code string, the first three letters are the initials of the fluid maker's name. The next five numerals denote the date on which the fluid was made. For example, fluid #1 was made on 8/25/89. The number following the date, "13" in this case, is the zeolite type (that is, a code number pertaining to the basic material of the particulate phase of the fluid.) The next letter, R, X, or T, is a unique serial identifier. "K", after the serial letter, indicates that the base material of the liquid phase is kerosene. The next set of numerals consists of two numbers, the first of which is the quantity of solid phase in grams and the second is the quantity of liquid phase, in cubic centimeters. "BM3DAYS" for fluid #1 stands for "ball milled for 3 days" while "25GMA" for fluid #3 stands for "25 grams of maleic anhydride"

**Table 4.1. Three kerosene based ER fluids**

| fluid | original names |
|---|---|
| #1 | TMF8258913RK20004000BM3DAYS |
| #2 | TMF8238913XK20004000 |
| #3 | TMF8298913TK500900(25GMA) |

During the processing of the fluids, the solids are measured in grams and the kerosene content in cc or ml. The specific gravity of kerosene is 0.8 while that of the particulates is 2.0. The specific gravities, s.g., of the composite ER fluids and their resulting percentage solid content are listed in Table 4.2. The fluids can be diluted to different solid contents by adding more kerosene.

**Table 4.2. Solid contents of the ER fluids**

| fluid | solid | liquid | s.g. | solid content |
|---|---|---|---|---|
| | [gram] | [cc] | | [% volume] |
| #1 | 2000 | 4000 | 1.04 | 20 |
| #2 | 2000 | 4000 | 1.04 | 20 |
| #3 | 500 | 900 | 1.061 | 21.74 |

## 4.2. Experimental Procedure

All of the data collection carried out in this study was carried employed the viscometer apparatus. Over several months, the experiments were divided into three phases.

In the first phase, all three fluids were tested to gain an initial characterization of their behavior. The viscometer was outfitted with two alternate torque transducers which exhibited largely differing values of rotational stiffness. When both transducers were employed in experiments covering a broad band of electrical excitation frequencies, a phenomenon involving rotational resonance of the cup-and-sensor assembly was identified and characterized (see Section 4.6). Over the wide frequency band, the time histories of voltage, current, and torque were recorded simultaneously in order to study wave forms, phase shifts, and other relationships (see Section 4.5).

In the second phase, the excitation signals were varied to cover cases of sustained, d.c. signals, sinusoidal waveform, and sinusoidal wave with off-set relative to zero. A measurement protocol was then developed for employing a sinusoidal wave, without offset, for use over a matrix of measurements in phase three (see Section 4.5). Also in the second phase, the effect of solid content was studied (see Section 4.8) resulting in selection of a specific gravity value near 1.0 (corresponding to approximately 17.5% solid by volume) for the remaining broad matrix of measurements.

In the third phase, the sinusoidal excitation protocol was employed for measurement of the response of the three fluid specimens over each of three main sets of tests. The first set involved measurements over a matrix of parameters covering the following conditions:

- 2 values of shear rate (17.3 and 173 1/s—where the shear rate units denote the velocity gradient across the fluid gap, mm per second per mm of gap,)
- 1 value of temperature (25 degrees C,)
- 8 values for imposed field frequency (2, 10, 30, 75, 100, 200, 500 and 1000 Hz) and,
- 9 levels of electric field strength (0., 0.5, 1.0, 1.5, 2.0, 2.5, 3.0, 4.0 and 4.5 kV/mm.)

For fluid #1, an additional shear rate value of (1.73 1/s) was used.

The second set of measurements focused upon the effect of shear rate, covering values of 0., 8.66, 17.3, 34.6, 69.3, 104, 139, 173, 260 and 346 1/s, for a single temperature value and field strength, and selected values for excitation frequency.

The third set of measurements was directed at the study of temperature sensitivities, examining temperature values of 16, 25, 50, 75, 100, 125 and 150 degrees C, for a single value of shear rate and selected values of field strength and excitation frequency. Additional temperatures levels were studied with fluid #1.

## 4.3. Rheological Models for ER Fluids

As a basis for discussion of the experimental results, it is useful first to lay out an elemental model for ER fluids. Reference will then be made to the terminology of the model and to its constituent formulation in fitting and interpreting the measured results.

There are mainly three rheological models that have been popularly considered for representing the mechanical properties of an ER fluid, as introduced below:

- the non-linear viscoplastic representation proposed by Gorodkin et al. (1975), as expressed by the relationship:

$$\tau^{1/n} = \tau_y^{1/n} + (\eta du/dy)^{1/r}$$

  where $\tau$ is the shear stress, $\tau_y$ the Bingham stress (effectively, the yield stress of the activated fluid responding as a solid,) $\eta$ the plastic viscosity, du/dy the shear rate, and n some constant.

- another non-linear approach, called the power law model, which is proposed by Stanway et al. (1989a) and is expressed by:

$$\tau = c_n\left(\frac{du}{dy}\right)^n$$

  where both $c_n$ and n are functions of the electric field strength.

- The third model is a more popular linear viscoplastic model defined by the relationship:

$$\tau = \tau_y + (\eta du/dy)$$

  which is also called the Bingham plastic fluid.

In this study, only the linear, or Bingham plastic fluid model is used in discussing experimental observations. A more complete constitutive equation for the Bingham plastic fluid is

$$\tau = \begin{cases} -\tau_y + \eta\dfrac{du}{dy} & \text{if } \dfrac{du}{dy} < 0 \\ \tau_y + \eta\dfrac{du}{dy} & \text{if } \dfrac{du}{dy} > 0 \end{cases}$$

or

$$\frac{du}{dy} = \begin{cases} \dfrac{\tau + \tau_y}{h} & \text{if } \tau < -\tau_y \\ 0 & \text{if } |\tau| \le \tau_y \\ \dfrac{\tau - \tau_y}{h} & \text{if } \tau > \tau_y \end{cases}$$

which is shown graphically in Fig. 4.1.

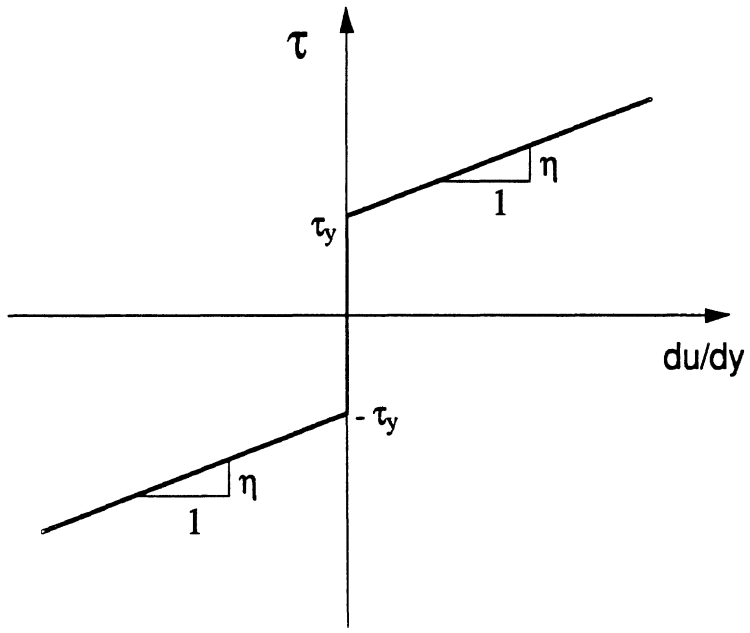


**Fig. 4.1 A Bingham plastic fluid.**

The Bingham plastic fluid model imposes the basic assumption that both the plastic viscosity, $\eta$, and the Bingham stress, $\tau_y$, are independent of the shear rate du/dy—an assumption which may not hold across all regimes of ER fluid behavior. For a given ER fluid, the Bingham stress $\tau_y$ is a function of the electric field strength, temperature, solid content, excitation frequency, and even the shear rate. Notwithstanding these complexities, the basic form of the bingham plastic model serves as a convenient discipline for discussing the data gathered in this study.

## 4.4. The Plastic Viscosity $\eta$

The Bingham plastic model defines a plastic viscosity, $\eta$, as the rate of change of shear stress per unit shear strain in the operating region following plastic yielding of the "solid" phase of the material. This viscous property was measured as a first step in the experimental process with each of the three prepare fluids, taking the case of zero electric field strength.

The base liquid, kerosene, was also characterized. Shown in Figure 4.2 are the data showing the three ER fluids plus kerosene. We note that the kerosene is essentially a Newtonian fluid having a very low viscosity (about 2.4 cP). With the addition of particulates to create ER fluids, however, we observe both qualitative and quantitative differences in the data, with no electric field applied. At a shear rate of 350 1/s, for example, the shear stress levels achieved by fluids 1,2,and 3 exceed that of kerosene by 14.8, 15.3, and 11.9 times, respectively. The ER fluids show a

behavior which is clearly non-Newtonian, exhibiting a pronounced shear-thinning behavior following an initially high slope of response. In these cases, any distinctions between plastic and viscous domains of behavior are blurry. Further, the stress vs. rate slopes vary continuously over the shear rate range from 0 to 100 1/s. Beyond du/dy values of 100, relatively constant viscosities appear.

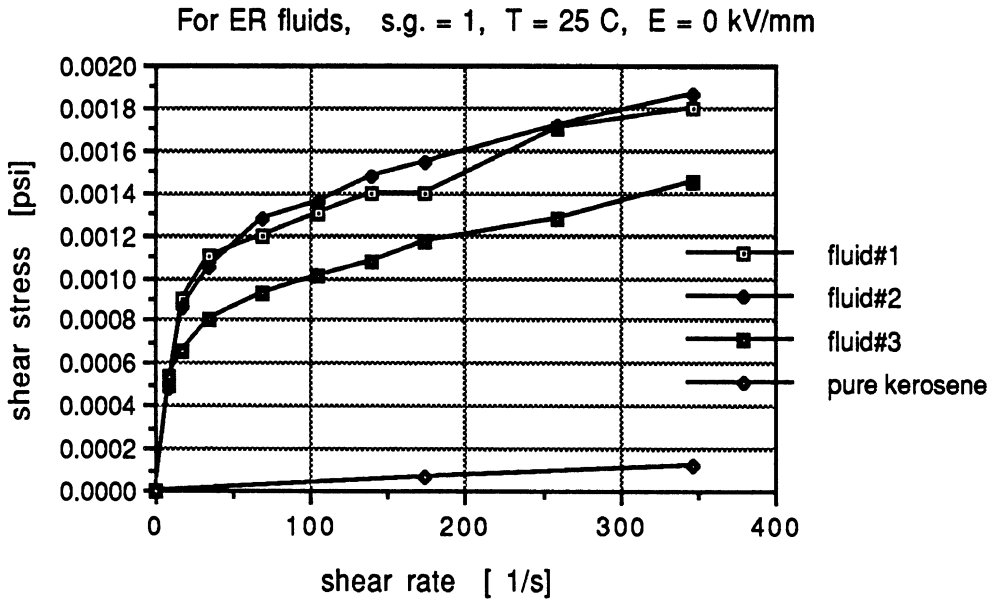


**Fig. 4.2. Base viscosity of ER fluids.**

Since the shear stresses observed here in the absence of an electric field are a couple of orders of magnitude smaller than those seen with strong fields applied, the non-linearities observed in Figure 4.2 may not have a significant effect on the applicability of the Bingham model.

While these ER fluid samples were all formulated to achieve a specific gravity value around 1.0, it is known that the zero-field viscosity will rise further when formulation are made at higher levels of solid content, and thus higher values of specific gravity.

## 4.5. Input and Output Wave Forms

Preliminary experiments were conducted simply to examine the shapes of the excitation and response waveforms which result from sinusoidal variation of the ER field voltage. For a fixed peak value of voltage, it was observed that the response to a low frequency sinusoidal wave involved virtually the same peak shear stress as resulted from a d.c. application of the same voltage. However, with d.c. electric fields, the ER fluid appeared to be non-stationary, with the particulate phase tending to forming clusters, and arcing across the fluid gap occurring more frequently. Some mass shift from one pole to the other under the d.c. field condition is suspected, although a well-controlled flow visualization study would be needed in order to study this phenomenon.

In a macroscopic sense, it is apparent that the ER fluids formulated here cannot distinguish between a positive- and negative-oriented field voltage. Thus, the viscosity arising in response to field condition can be described by a scalar quantity which changes magnitude equally with positive- and negative-going voltages. As a result, the ER fluid viscometer (which simply rotates continuously in the same direction) responds to a symmetric sine wave of electric field voltage by exerting a torque whose waveform looks more or less like a rectified sine wave at the torque transducer. This rectification provides a harmonic time history of torque whose fundamental component is at a frequency which is twice that of the excitation sine wave.

Fig. 4.3 shows a segment of recorded test data illustrating this response. The electric excitation voltage is a symmetric sine wave at 10 Hz, swinging to equal peak values in the positive and negative directions. The signal produced by the torque sensor, in turn, demonstrates a single-polarity signal, more rounded than a true rectified sine wave, and indeed closely approximating a sine wave, itself, at a frequency which is twice the field excitation frequency. The "rounding" effect appears to be due to a nonlinearity in the influence of field strength on the viscosity of the ER fluid, with a particularly weak ER response arising at low field strengths as illustrated explicitly, below.

Under the excitation of a sinusoidal field voltage, then, the torque response signal can be approximated by two components—a pure sine wave and a d.c. part which is equal to the time average of the total wave. A so-called "peak torque value" is employed in reporting much of the experimental data from this study, derived from the sum of the time average (or d.c. component) and the single amplitude value describing the quasi-sine torque signal. The amplitude of the torque wave is calculated using the r.m.s (root mean square) values measured through a spectrum analyzer. The d.c. signal is measured directly off a voltmeter.

The current is also monitored and measured using the spectrum analyzer.It is also evident from Figure 4.3 that minimal phase shift exists at this low frequency, among the torque, voltage and current signals. Clearly, the ER circuit posed by the fluid and the cup/bob device constitutes only a resistive load at the 10 Hz excitation. At higher frequencies, a much larger part of the current is required to charge the cup/bob capacitor, resulting in marked phase shifts, with the capacitive current leading the voltage by 90 degrees.

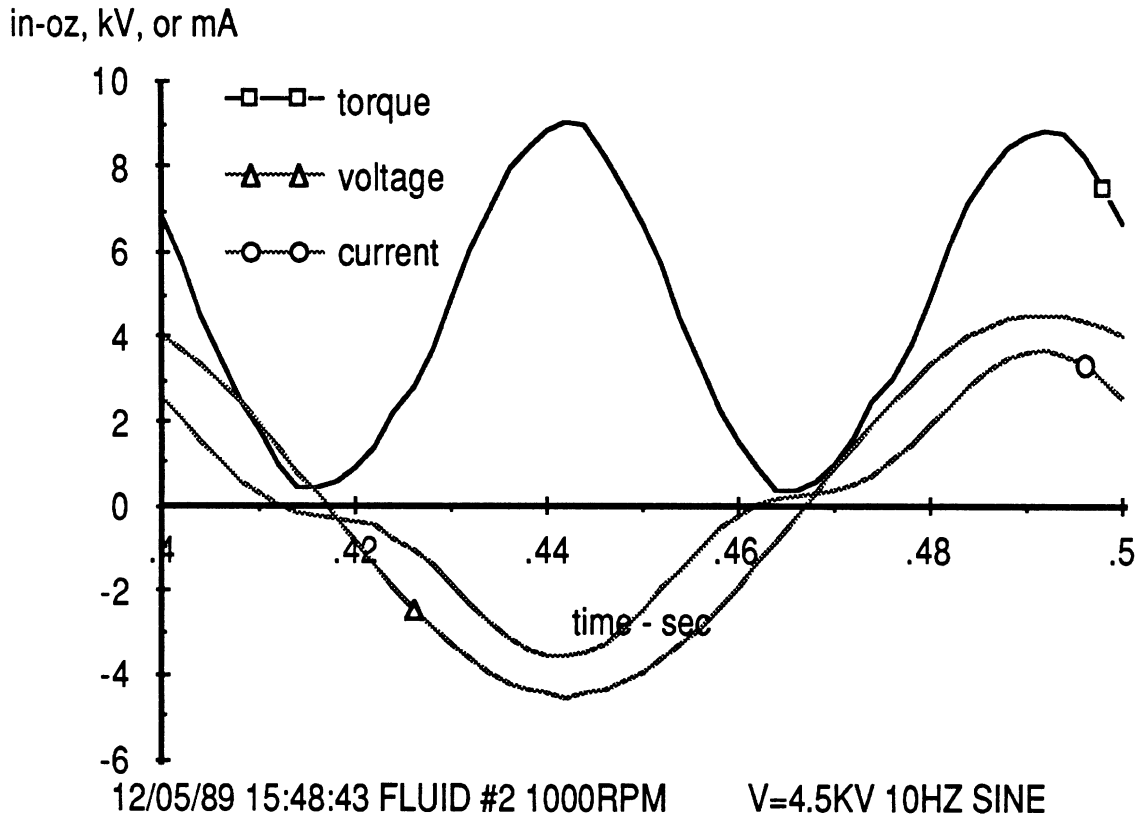


**Fig. 4.3. Wave forms of torque, electric field voltage, and current.**

Shown in Figure 4.4 is a plot—using data from many cycles of the viscometer—of the response torque, on the horizontal axis, and both field current and field voltage on the vertical axis. The figure shows that, near zero voltage, the torque response is quite weak (showing a small slope, $\partial$torq/$\partial$volts). This low-gain portion of the torque curve accounts for the rounding in the torque time history seen in Figure 4.3, in response to a symmetric sine wave of field voltage. Figure 4.4 also indicates that the current relates to response torque in a rather linear fashion. Further, the current levels exhibited by these non-water-based fluids is of low magnitude.

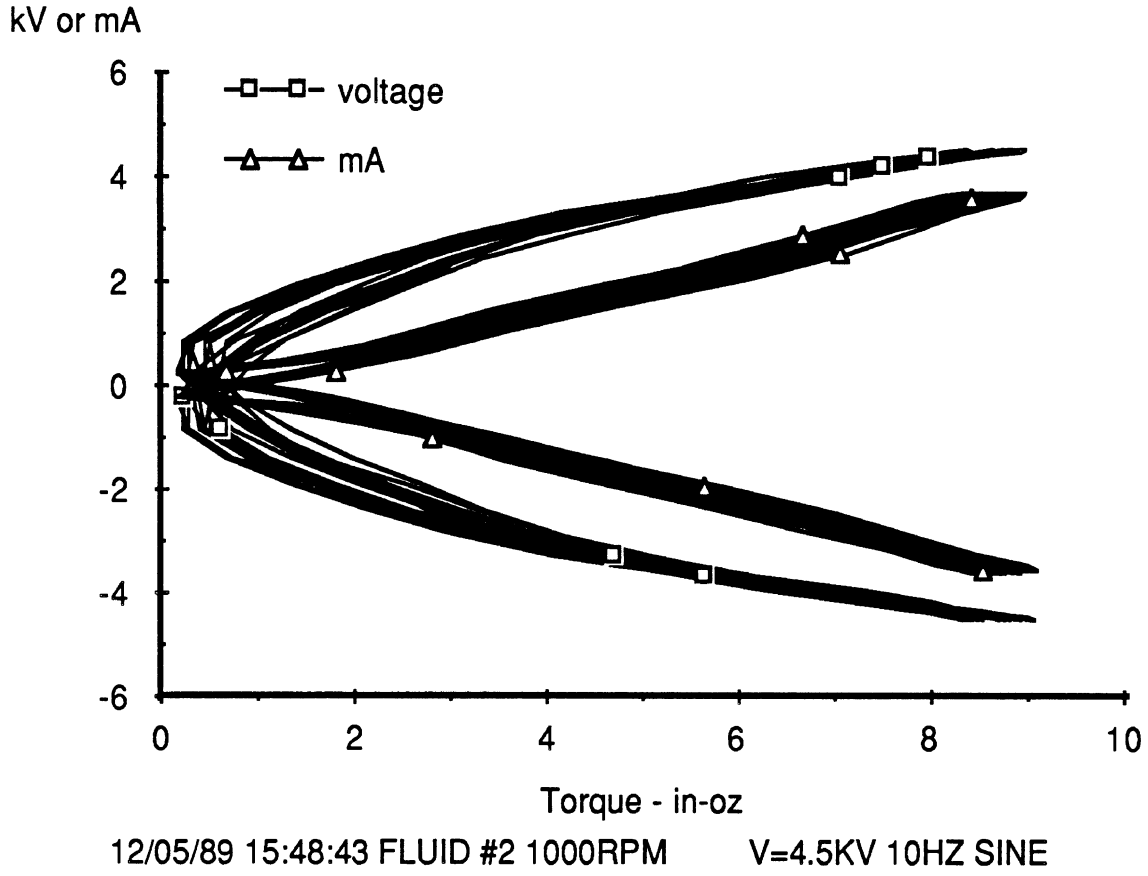


**Fig. 4.4. Relation between the current or voltage and the viscometer torque.**

## 4.6. Examination of Resonance in the Cup-and-Torque Sensor System

A rheometer or viscometer is a basic tool used to characterize the rheology of a fluid. In a conventional use of such devices, the test proceeds under effectively steady state conditions. However, when an ER fluid is tested over a broad band of excitation frequencies, one will inevitably encounter the mechanical resonance in the rotational mode of vibration of the cup mass supported by the torque transducer. Clearly, the cup-and-torque sensor system constitutes a second order system whose natural frequency, $\omega_n$, is determined by the mass moment of inertia of the cup, I, and the torsional stiffness of the sensor, $k_t$, per the relationship,

$$\omega_n = \sqrt{\frac{k_t}{I}}$$

and the damped natural frequency of this system is,

$$\omega_d = \omega_n \sqrt{1 - \zeta^2}$$

where $\zeta$ is the damping coefficient, calculated using the following equation:

$$\zeta = \frac{C}{2\omega_n I}$$

In the above equation, C is some constant which is linearly related to viscosity of the ER fluid.

In the viscometer apparatus assembled here, a light-weight cup was employed so as to minimize the rotational moment of inertia, and thus elevate the resonant frequency. As for the sensor, the stiffness is limited by the minimum rotation or strain which is required to generate suitable signals in the sensing bridge. Two torque sensors were employed in an initial examination of the resonance issue. A strain-gage type transducer manufactured by Lebow, Inc. provided a torsional spring constant of 364 Nm/rad, while a semiconductor-type transducer from Keys, Inc. provided twelve-fold increase in spring constant, to 4516.3 Nm/rad. With the same mass moment of inertia in both systems, the undamped natural frequency computed with the Keys transducer was approximately 3.5 times that obtained with the Lebow transducer. (One disadvantage with the Keys transducer was the large extent of zero shift which is common with semiconductor bridges.)

Figs. 4.5 and 4.6 show the dynamic responses measured with each of the two torque transducers, using ER fluid #3. The legends "maximum" and "minimum" refer to the maximum and minimum torque values measured in a cycle. The data clearly show the behavior which is characteristic of a damped second order mechanical system. Note, especially, that the anomaly of negative polarity torques is seen in the vicinity of resonance even through the discussion above establishes that the torque delivered from the fluid shear mechanism is always of one (positive) polarity, as determined by the direction of rotation of the viscometer. Further, the resonant peaks rise well above the level seen throughout the rest of the examined spectrum.

Clearly, the resonant amplification in response does not imply any resonating property in the rheological response of the ER fluid since the same fluid shows dramatically differing results in the two system configurations. Rather, these results confirm the hypothesis that mechanical resonances in a viscometer-type device will serve to distort the apparent torque response obtained using ER fluids over a broad band of excitation frequencies. In the example case, resonance was observed at response frequencies (i.e. twice excitation frequencies) of 130 and 570 Hz—approximating the ratio of damped natural frequencies that one computes for the system with the two respective torque transducers installed.

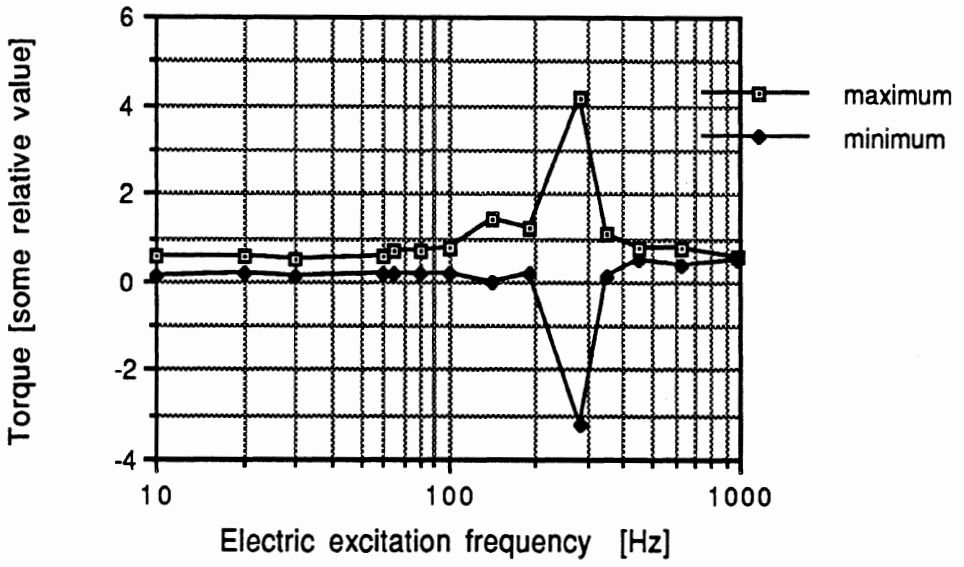


**Fig. 4.5. The dynamic response using the Keys transducer.**

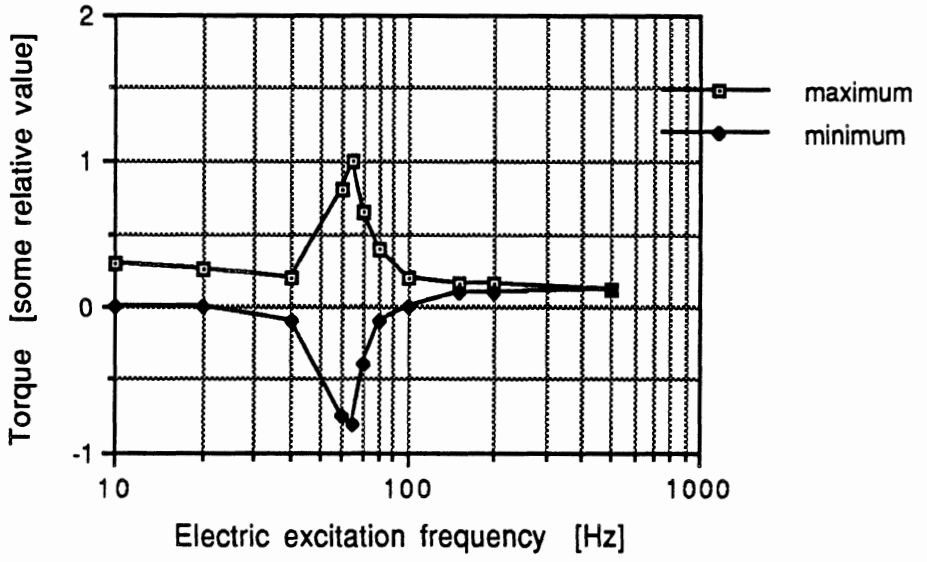


**Fig.4.6. The dynamic response using the Lebow transducer.**

As far as the authors know, no serious discussion about the issue of viscometer dynamics is reported although similar resonances in engine mounts and dampers are reported by many investigators (Duclos et al., 1988; Shoureshi et al., 1986; Shul'man et al., 1987a; Shul'man et al., 1987b; Stanway et al., 1985; Stanway et al., 1989b; Stevens et al., 1984).

Since it is not feasible to build a viscometer or rheometer having a natural frequency which exceeds the range of interest with ER fluids, it is simply necessary that dynamic measurements be interpreted with great care, especially around the resonance region. As a long-term solution to this

issue, the measured torque data must be processed using an inverse transformation characterizing the dynamic system, quite apart from the transfer function characterizing the ER fluid's response. Such a dynamic characterization was not undertaken during the present study.

Notwithstanding the need for precautions in the interpretation of dynamic viscometer results, the authors note that the d.c. component of the torque signal in the high frequency region offers a crude indicator of the extent of ER fluid response to field excitation. That is, if a measurable d.c. signal component is still observed, even in the 1-2 kHz region for example, it implies that a sine wave of torque response is present, biased above zero as discussed above, and yielding an average value which is manifest as the d.c. component. Due to the nonlinearity in viscosity, however, no close-form analytical determination of the implied sine wave amplitude is available.

Following the tests shown in Figs. 4.5 and 4.6, the cup wall thickness was reduced further to cut down the total mass while a heating mat, which causes a certain mass increase, was added to the cup in order to provide for temperature control. The net effect of these changes was to increase the natural frequency with the Lebow transducer to approximately 150 Hz. The majority of the tests reported in this study were carried out with the thin-wall cup and the Lebow transducer.

## 4.7. The Bingham Stress $\tau_y$ as a Function of the Electric Field Strength

The fluids in question are called electro-rheological because their Bingham stress $\tau_y$ changes in response to electric field strength. Two basic models have been proposed to describe this dependency.

The first of such models is as shown in Fig. 4.7 where the electro-rheological effect appears when the electric field strength E is greater than a certain threshold value, Ec—typically equal to approximately 1 kV/mm (Brooks, 1982)—and beyond which threshold the Bingham stress is linearly related to the magnitude of the field strength (Brooks, 1982; Stangroom and Eckersley, 1985). Mathematically, this model is expressed by the relationships,

$$\tau_y = \alpha(E-Ec) \qquad \text{when } E \geq Ec$$

$$\tau_v = 0 \qquad \text{when } E < Ec$$

where $\alpha$ is some constant.

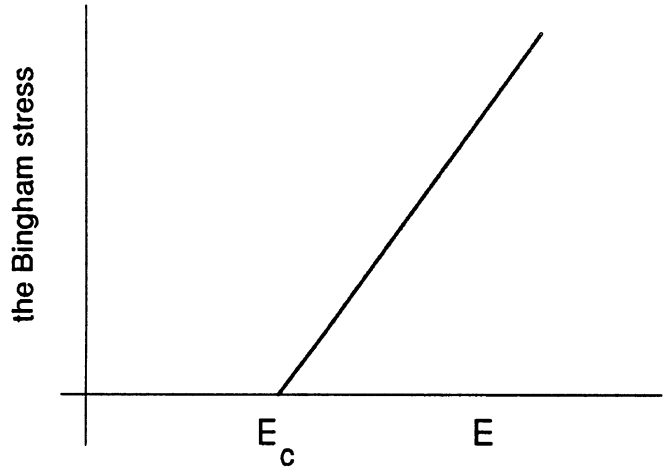


**Fig. 4.7. electro-rheological model with a threshold field strength.**

The second electro-rheological model can be mathematically expressed as

$$\tau_y = \Phi E^n$$

thus

$$\tau = \Phi E^n + \eta \frac{du}{dy}$$

where $\Phi$ has been called the Winslow number, and n is some constant. A commonly-cited value for n is 2 (Phillips, 1969; Uejima, 1972).

The suitability of these two models is considered here in the light of the experimental data gathered using the ER fluids prepared for this study. Figs 4.8, 4.9 and 4.10 show the basic electro-rheological behaviors measured for fluids #1, #2 and #3, respectively. Obviously, no linear dependence of shear stress on electric field strength is observed. Further, with no threshold sensitivity to field strength, the first model discussed above does not seem applicable.

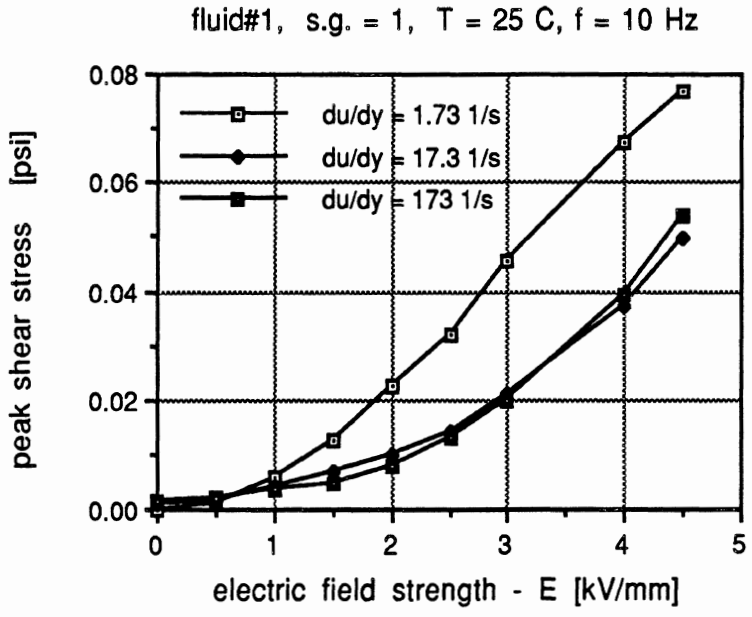


**Fig. 4.8. electro-rheological effect on fluid #1.**

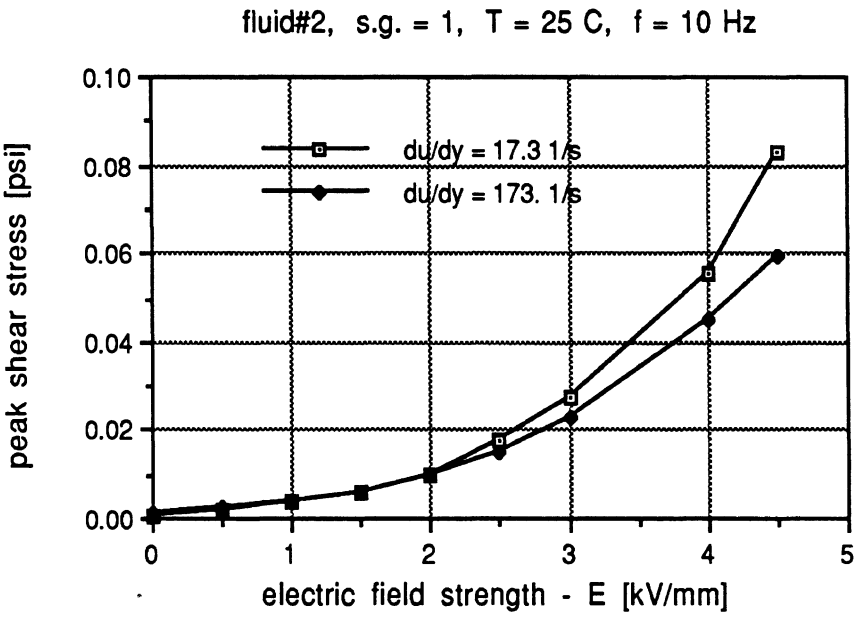


**Fig. 4.9. Electro-rheological effect on fluid #2.**

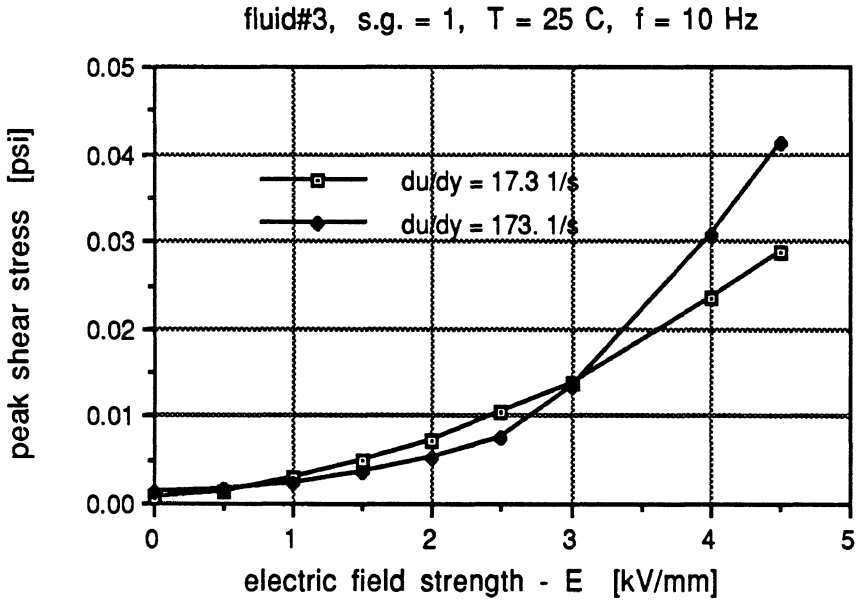


**Fig. 4.10. Electro-rheological effect on fluid #3.**

Considering the second model, the power law type, with n = 2.5, we obtain the curve fits as shown in Figs. 4.11 and 4.12. These data show that very good agreement can be obtained, although we recognize that different fluids and different values of shear rate may have different values for the coefficients as well as the exponent.

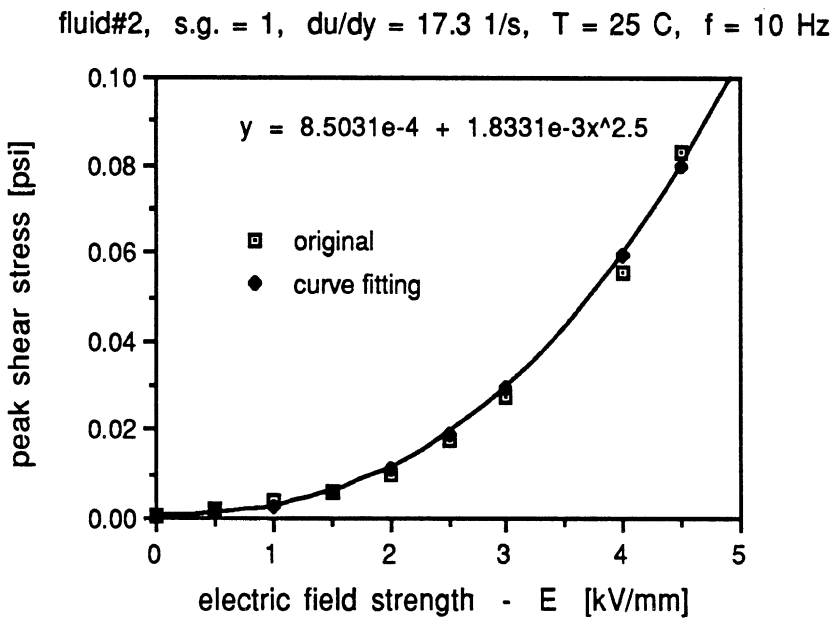


**Fig. 4.11. Curve fitting for fluid #2 at 17.3 1/s.**

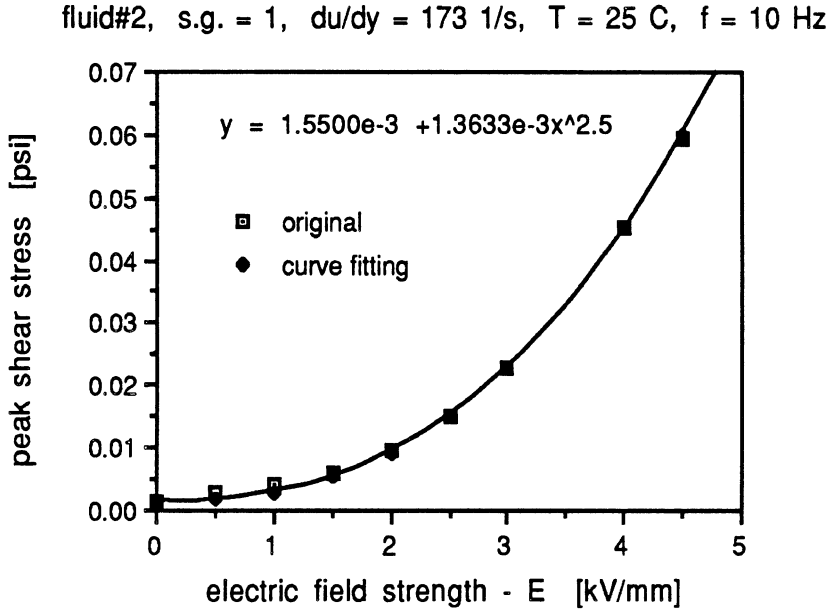


**Fig. 4.12. Curve fitting for fluid #2 at 17.3 1/s.**

Looking at Figs 4.8, 4.9 and 4.10, for the same test conditions (s.g., temperature, frequency, and the shear rate), one would conclude that fluid #2 offers the best performance as far as the absolute value of the shear stress is concerned. Fluid #1 is the next in the line, and fluid #3 provides the lowest levels of shear stress. The highest shear stress value for fluid #2 within the test range is just over 0.08 psi. However, with a higher solid content and a higher electric field strength, a higher shear stress level can be achieved.

## 4.8. Influence of the Concentration of Solids

It seems a straightforward hypothesis that the effectiveness of an ER fluid is dependent on the solid content s.c., which is the amount of particulates as a percentage of total volume. Figs. 4.13 and 4.14 show the electro-rheological behavior of fluid #1 at different levels of solid concentration. Here, the specific gravity of the ER fluid s.g., is used as an easily-measured value for expressing the solid content. The specific gravity is linearly related to the solid content in the following manner

$$s.g. = s.g._s \cdot s.c. + s.g._l \cdot (1 - s.c.)$$

or

$$s.c. = \frac{s.g. - s.g._l}{s.g._s - s.g._l}$$

where $s.g._s$, $s.g._l$, and s.g. are the specific gravities of the solid, liquid phase and their mixture, respectively. Pure kerosene has a specific gravity of 0.8 while the solid particulates have a specific gravity of 2.0. Values of 0.8 and 2.0 for s.g. correspond to the conditions of pure kerosene and 100% solid, respectively. An s.g. value of 1.01 in Fig. 4.13 corresponds to a mixture having 17.5% of the total volume occupied by solid particulates.

Overall, the shear stress is seen to increase with the solid content, as reported qualitatively by Duclos et al. (1988). Fig. 4.13 shows that the shear stress follows a power law relationship as a function of electric field strength, with differing gains depending upon solid contents.

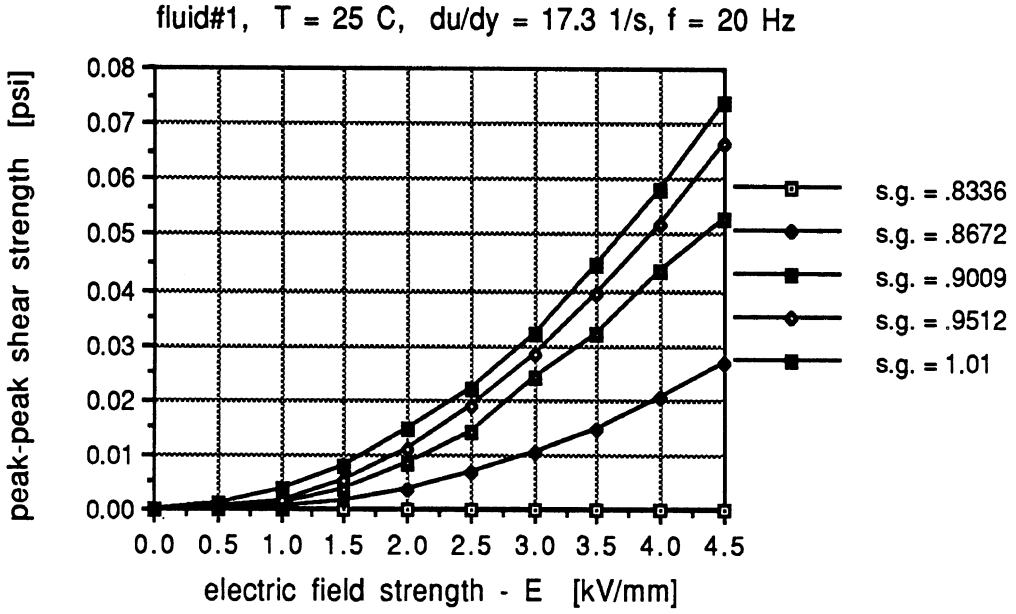


**Fig. 4.13 Electro-rheological behavior at different solid contents.**

In Figure 4.14, with peak shear stress plotted against the specific gravity value, we see that the ER effect is first observable at the 0.87 level of s.g.and becomes well developed when s.g. is at or above 0.9.

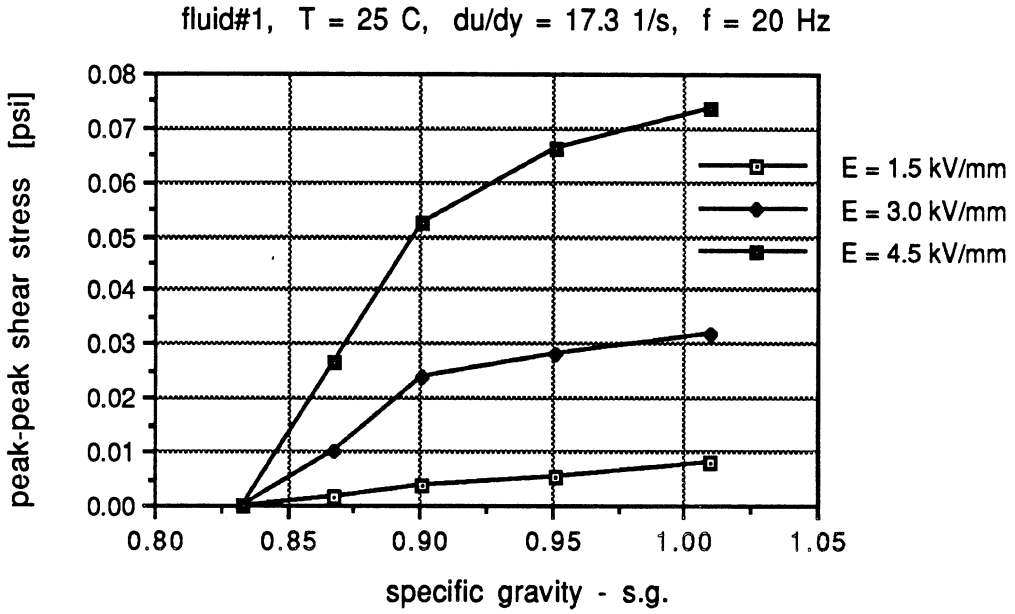


**Fig. 4.14. Electro-rheological behavior at different solid contents.**

The bulk of the tests in this study was completed using an s.g. value of 1.0, thus providing a consistent concentration to allow the study of other parametric influences. While it is clear that higher shear stress levels can be achieved with high percentages of solid content, the higher concentrations tend to entrain bubbles more readily and pose a higher value of base viscosity.

## 4.9. The Current Density

One of the main parameters of practical importance is the current density, which is defined as electric current per unit area, (mA per sq.mm.) A high level of current density implies a large current drain on the power supply and a high level of heat generation in the fluid. In this study, both the output voltage $V_{out}$ and the current $I_{out}$ delivered by the supply amplifier were measured. In some cases, the phase shift $\varphi$ between $I_{out}$ and $V_{out}$ was also measured. The electric circuit comprised by the viscometer apparatus can be approximated as that in Fig. 4.15. $I_{out}$ is the total output current and $V_{out}$ is the voltage from the amplifier. C represents the capacitance of the bob-cup assembly in the viscometer (or that of the valve plates in the valve-test apparatus.) R is the resistance across the fluid medium in the cup or the valve.

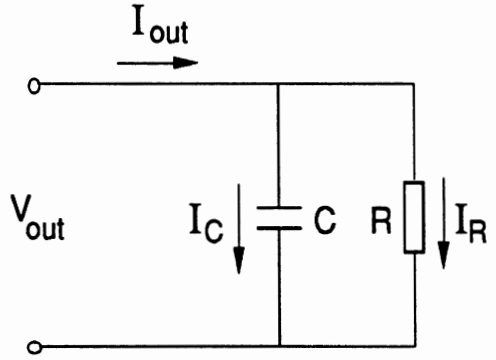


**Fig. 4.15. The electric circuit of an test device.**

If the voltage is a sinusoidal wave described by,

$$V_{out} = V_0 \sin \omega t$$

then the currents through the capacitor and resistor are, respectively,

$$I_C = I_{0C} \cos \omega t = \omega C V_0 \cos \omega t$$

$$I_R = I_{0R} \sin \omega t = R V_0 \sin \omega t$$

where $I_R$ is in phase with the voltage wave while $I_C$ is 90 degrees ahead of the voltage wave. The total current, $I_{out}$, is the sum of $I_C$ and $I_R$

$$I_{out} = I_0 \sin(\omega t + \varphi)$$

where

$$I_0 = \sqrt{I_{0C}^2 + I_{0R}^2} = V_0 \sqrt{(\omega C)^2 + R^2}$$

$$\cos \varphi = \frac{R}{\sqrt{(\omega C)^2 + R^2}} = \frac{I_{0R}}{I_0}$$

In this study, $I_0$ and, in some cases, $\varphi$ were measured. In the case where $\varphi$ was measured, the conductive current $I_{0R}$ can be calculated using the following equation:

$$I_{0R} = I_0 \cos \varphi$$

Theoretically, $\varphi$ can be calculated given R, C, and $\omega$. However, R and C are not constants in the ER fluid circuit. R generally decreases as the electric field strength increases and may be dependant upon frequency. The dielectric constant of either an ER fluid or pure kerosene, and thus its capacitance C, is also a function of frequency. There even exist some inductive wire connections which may have significance at higher frequencies, as well as other minor capacitors and resistors in a complete circuit.

Figs. 4.16, 4.17 and 4.18 show, for both fluid #3 and pure kerosene, the ratios of the in-phase or conductive current (equal to cos $\varphi$) over the total current. Fig. 4.18 is mainly to expand Fig. 4.17 in the low frequency region. The data show that the ratio tends to increase at higher frequencies and that the proportion of conductive current increases with voltage. Further, the

current through an ER fluid is much higher than that through kerosene. Clearly, the phenomena determining the respective current components are complex, although at frequencies below 10 Hz or so, $I_{out}$ is roughly equal to $I_{0R}$.

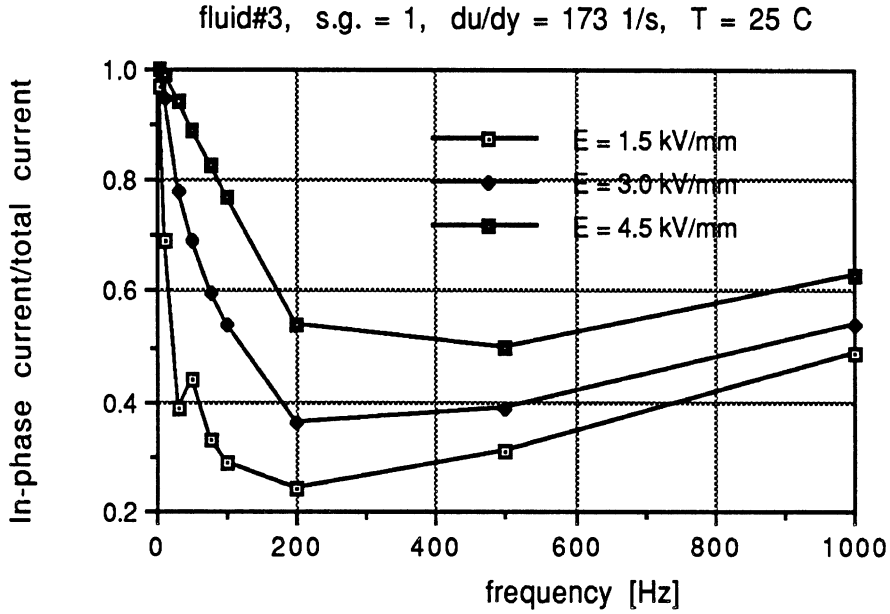


**Fig. 4.16. cos φ for fluid #3.**

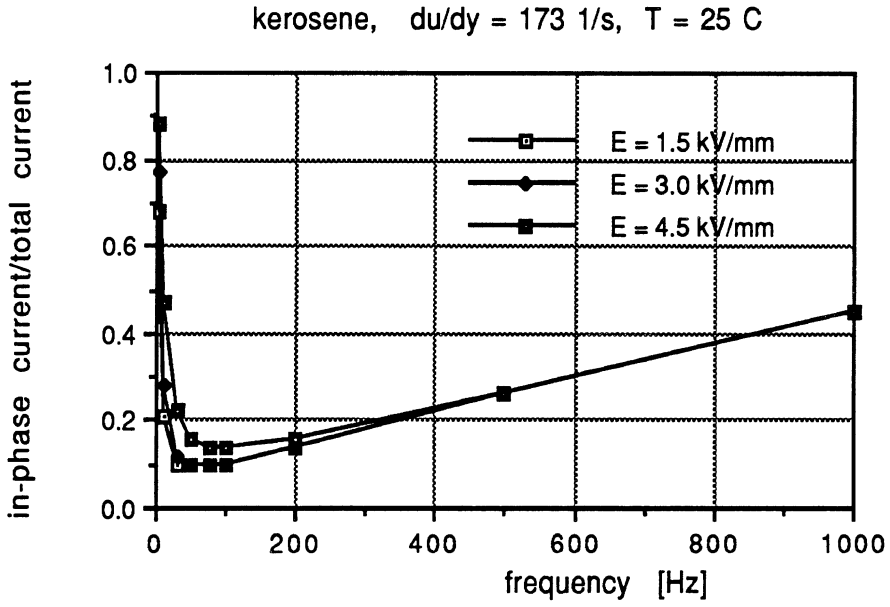


**Fig. 4.17. cos φ for kerosene.**

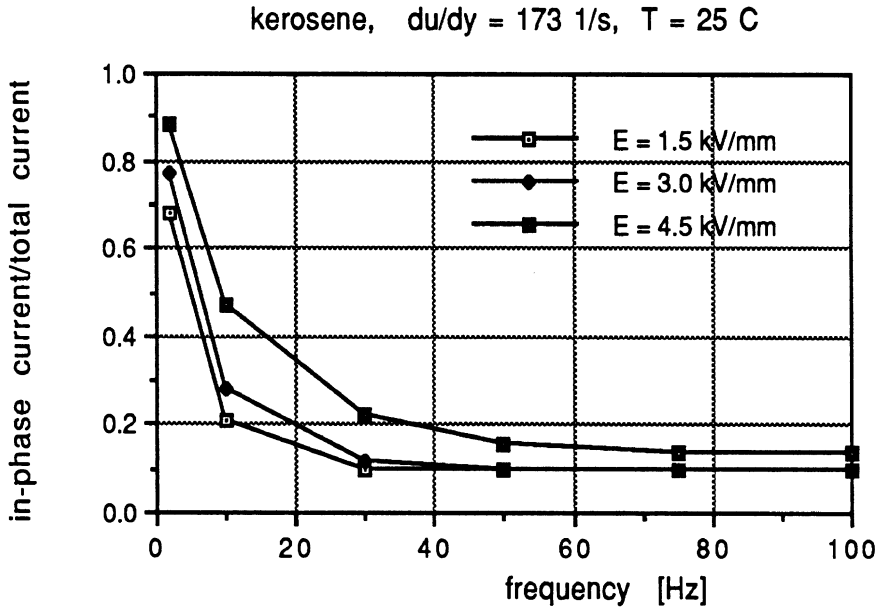


**Fig. 4.18. cos φ for kerosene.**

The current density data for the ER fluids in this study are shown in Figs. 4.19, 4.20, and 4.21. The excitation frequencies are all at 10 Hz, at which the currents are predominantly conductive. These curves are very similar to the power law functions relating shear stress to field strength, seen earlier, confirming again that the conductive current in the ER fluids is approximately linearly related to the shear stress under a given value of shear rate. Among all three fluids, fluid #3 has the lowest current density and fluid #1 has the highest.

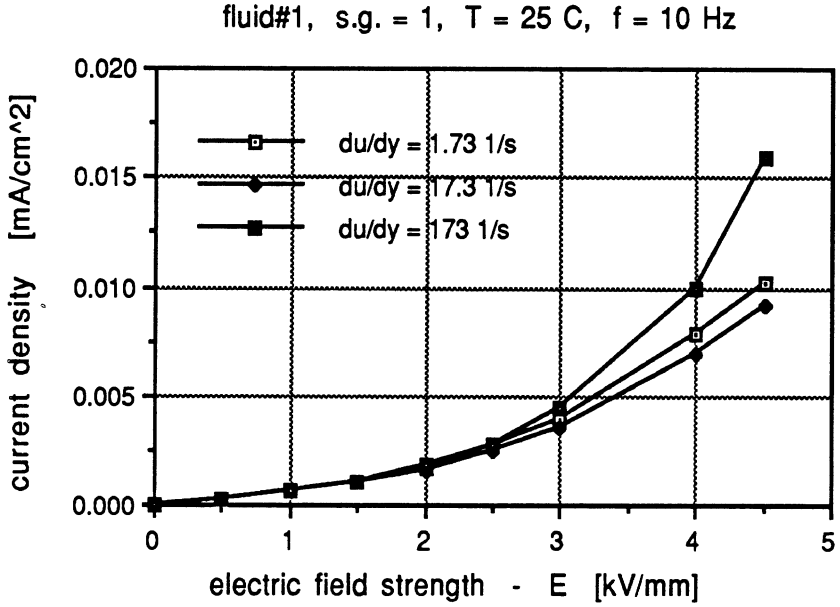


**Fig. 4.19. The current density for fluid #1.**

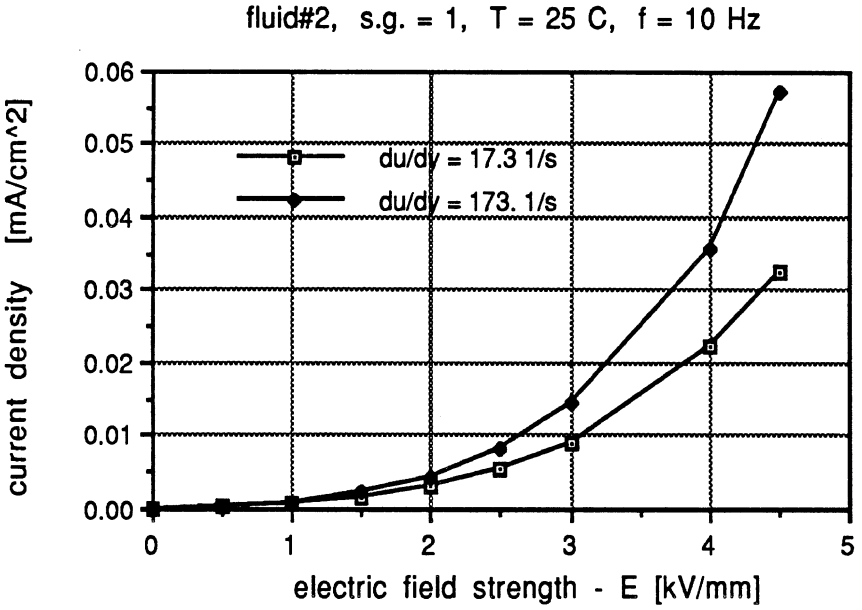


**Fig. 4.20. The current density for fluid #2.**

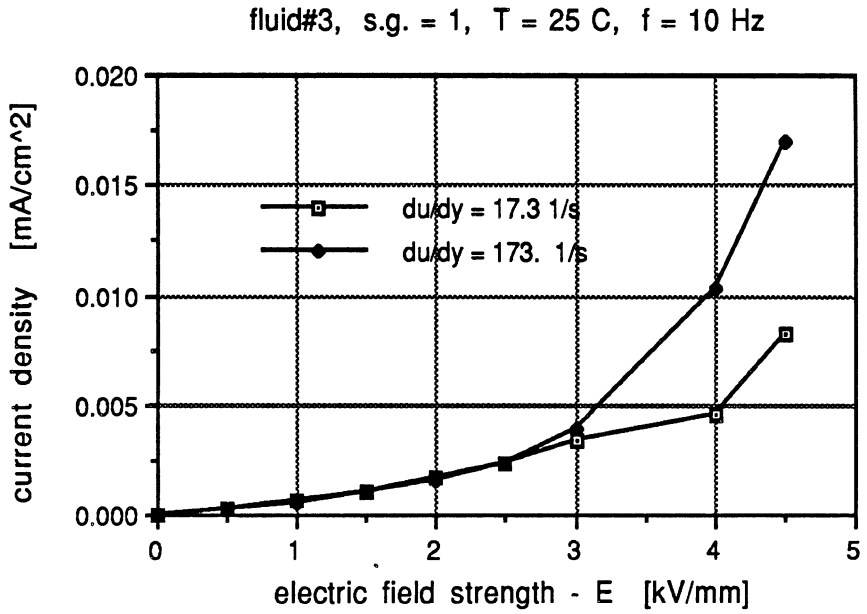


**Fig. 4.21. The current density for fluid #3.**

## 4.10. Effect of the Shear Rate

The three fluid samples were tested over the range of shear rate values from 1.73 to 346.3 1/s. As observed in Fig. 4.22, with average shear stress data plotted vs. shear rate at excitation frequencies of 10 and 30 Hz, we observe that fluid #1 does not exhibit the response of a perfect Bingham plastic fluid. Rather, the average shear stress decreases irregularly with shear rate, (as had been determined also in original experimental measurements conducted on the three fluids by

Filisko (1989).) Figs. 4.23 and 4.26 show the shear stresses vs. the shear rate for fluid #2 and fluid #3, respectively, under 10 Hz excitations. These data show more regular functional forms than seen with fluid #1, but still indicate decreasing shear stresses with shear rate.

Other investigators have reported sensitivities to shear rate which follow these general trends. For example, Bullough (1988) reported very high total shear stresses in an ER clutch at low shear rate. Massey (1971) reported a valve hysteresis effect near zero flow point. An anonymous study reported that the Bingham stress in a water-based ER fluid decreases as the shear rate increases. Stangroom (1983) and Stangroom and Eckersley (1985) simply take the position that there are two Bingham stresses, static and dynamic, and that the static Bingham stress is higher than the dynamic level for a given field strength. A common hypothesis has been that the decline in shear stress with shear rate may be attributed to the fluid's inability, with increasing shear rate, to sustain the relatively stable chains of particulates that otherwise prevail under near-static flow conditions.

As shown in Figs. 4.24 and 4.27, the current density response is seen to be relatively unaffected by shear rate, although differences are apparent between the two fluids.

Figs. 4.25 and 4.28 show the curious insensitivity of shear stress to shear rate when the field strength is varied sinusoidally at 1000 Hz. Similarly, the current density is very stable (Fig. 4.29). A possible reason for the insensitivity of shear stress at this high frequency condition is that the agitation of the particulate due to the 1 kHz excitation creates motions at the microscopic level whose velocities substantially exceed the shear velocities imposed mechanically in the experiment. Thus, the additional disturbance posed by the variations in shear rate is inconsequential to the bulk rheology of the fluid under this field variation.

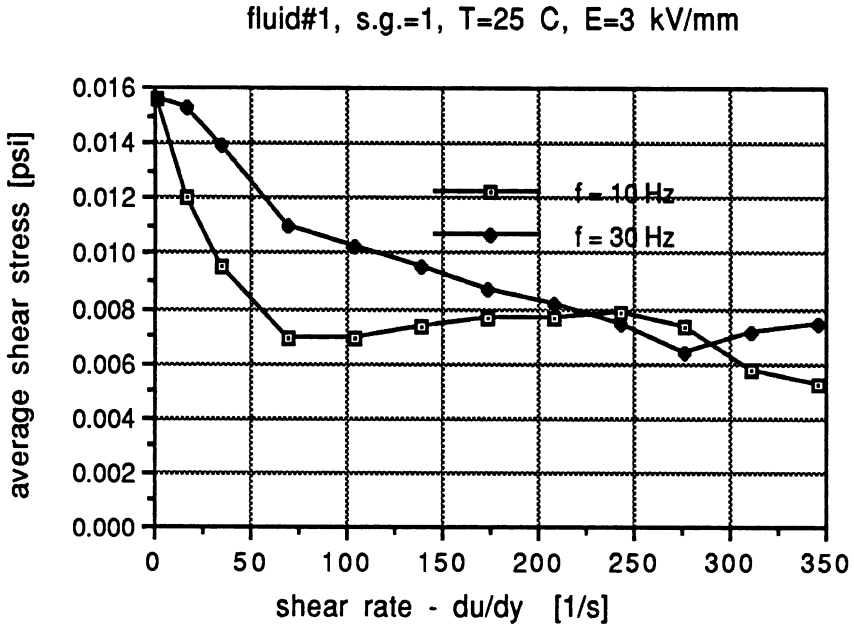


**Fig. 4.22. The shear stress vs. the shear rate for fluid #1.**

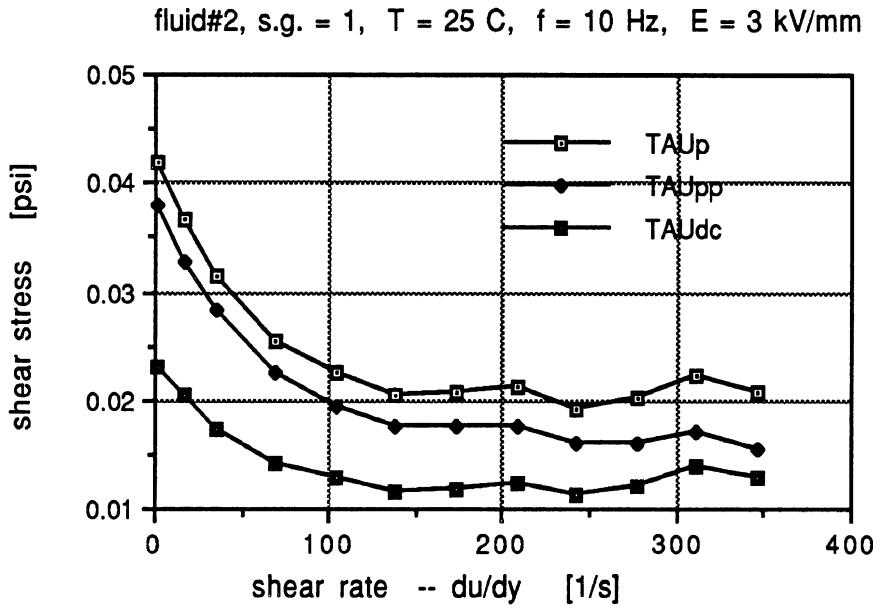


**Fig. 4.23. The shear stress vs. the shear rate at 10 Hz for fluid #2.**

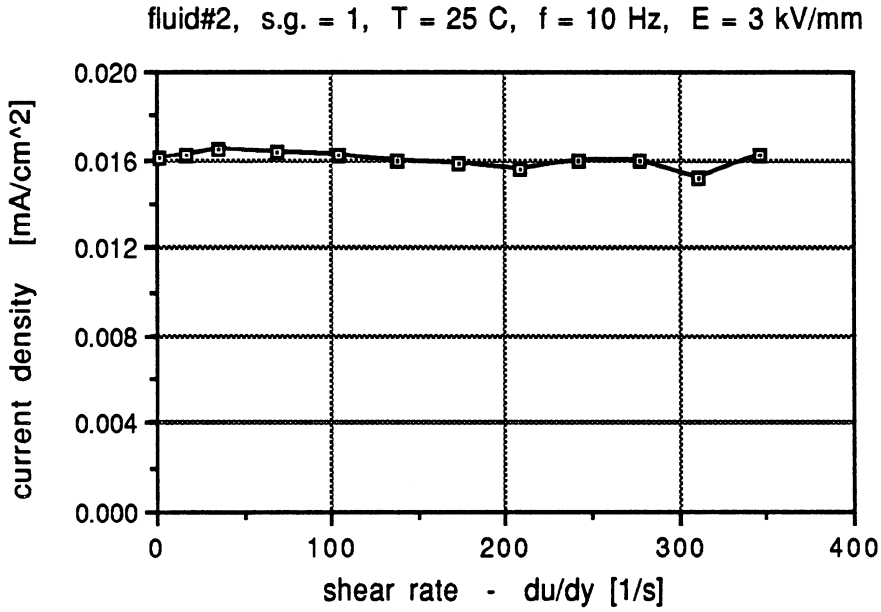


**Fig. 4.24. The current density vs. the shear rate at 10 Hz for fluid #2.**

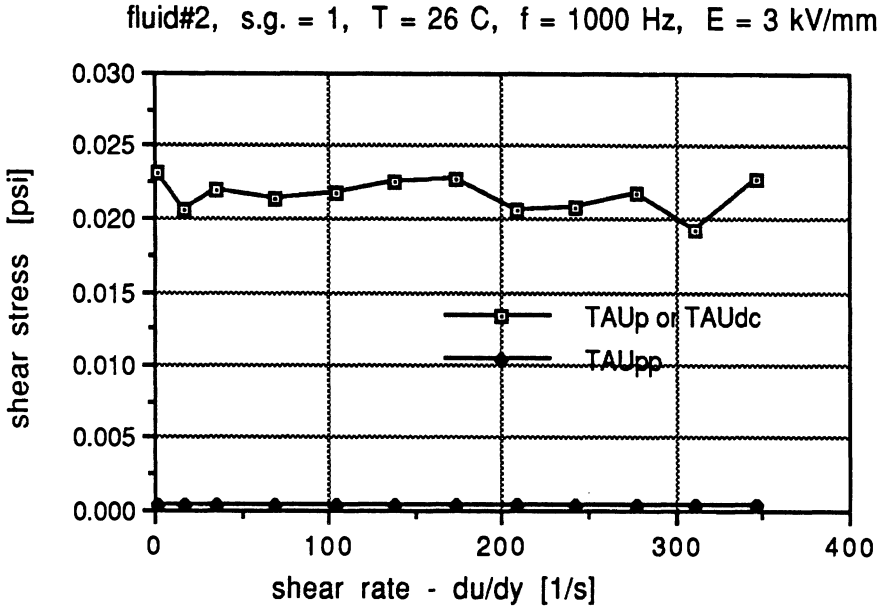


**Fig. 4.25. The shear stress vs. the shear rate at 1 kHz for fluid #2.**

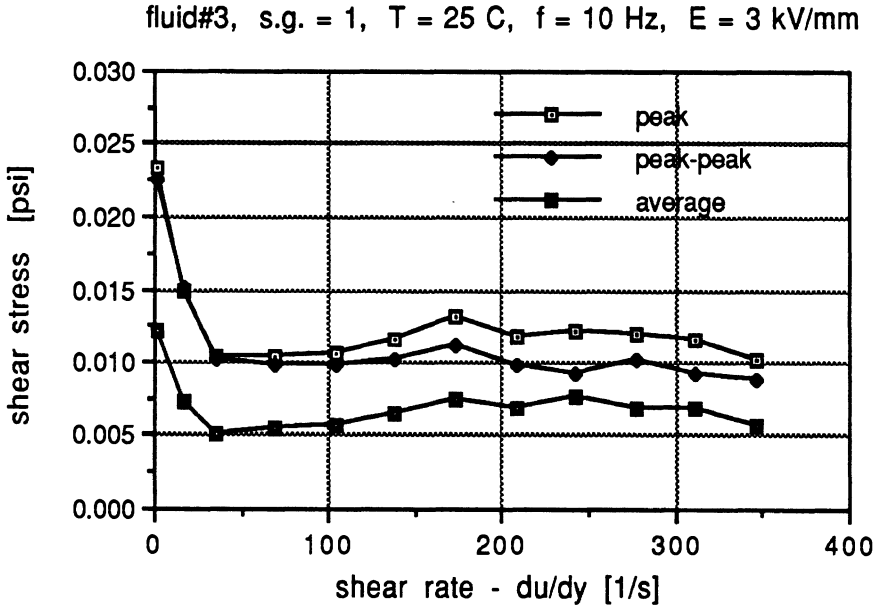


**Fig. 4.26. The shear stress vs. the shear rate at 10 Hz for fluid #3.**

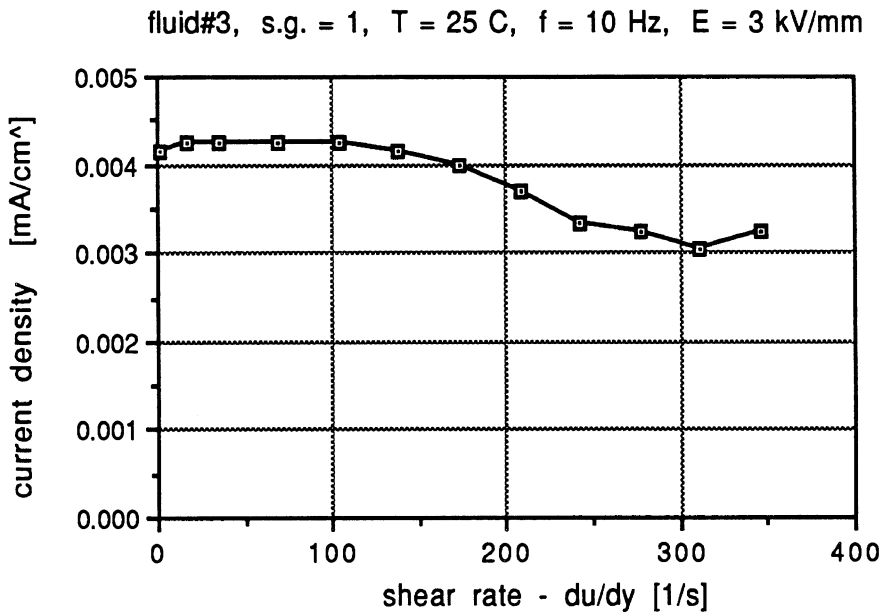


**Fig. 4.27. The current density vs. the shear rate at 10 Hz for fluid #3.**

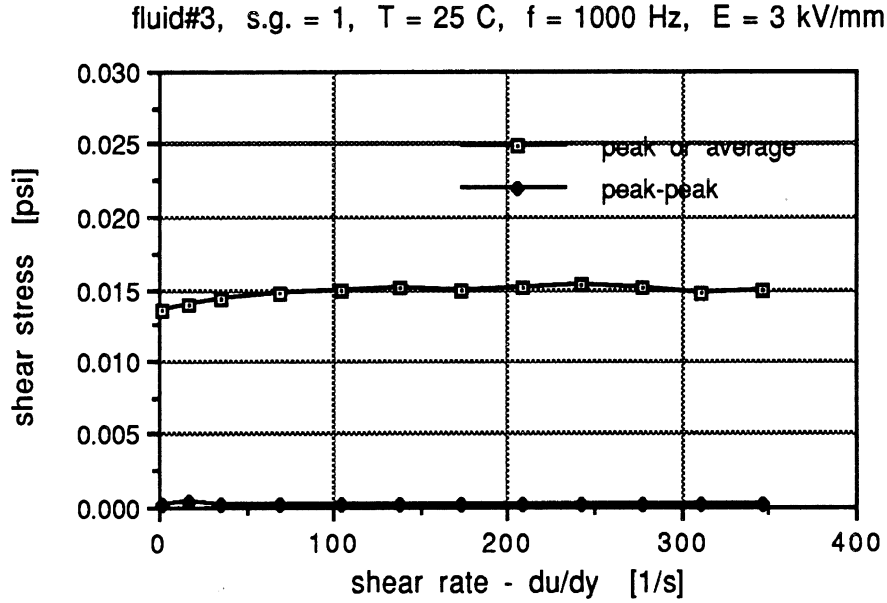


**Fig. 4.28. The shear stress vs. the shear rate at 1 kHz for fluid #3.**

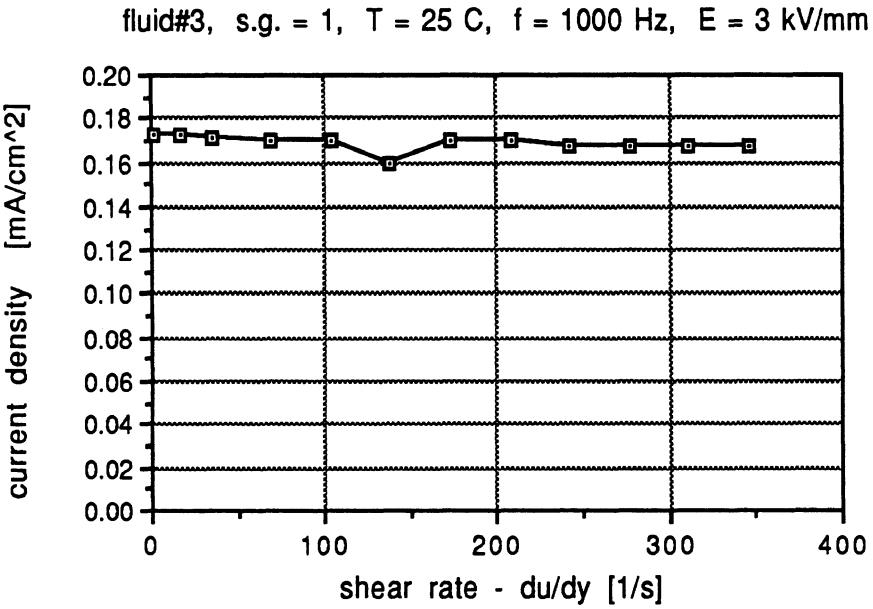


**Fig. 4.29. The current density vs. the shear rate at 1 kHz for fluid #3.**

## 4.11. The Bandwidth of the ER Fluids

Figs. 4.30, 4.31, and 4.32 show the time-averaged shear stress vs. electric excitation frequency for fluids #1, #2, and #3, respectively. Again, the reader should note that the shear stress or torque response frequency is twice that of the electric excitation, although the electrical excitation frequency is the plotted variable. At 1 kHz, all three fluids show substantial levels of average shear stress and the response levels are actually higher than those in lower frequency range. In fact, we have observed such responses even at excitations of 2 or 3 kHz. However, a finite level of d.c. shear stress at 1 kHz does not necessarily confirm a continuous response bandwidth of 1 kHz. As discussed earlier, a complete characterization of the inverse transformation of the dynamic test system will be needed to adequately study the high frequency end of the spectrum. In addition to the high-end mechanical attenuation which such a characterization would address, we would also deal with the irregularities seen in the middle frequency range of these data, which may also be caused by mechanical resonances.

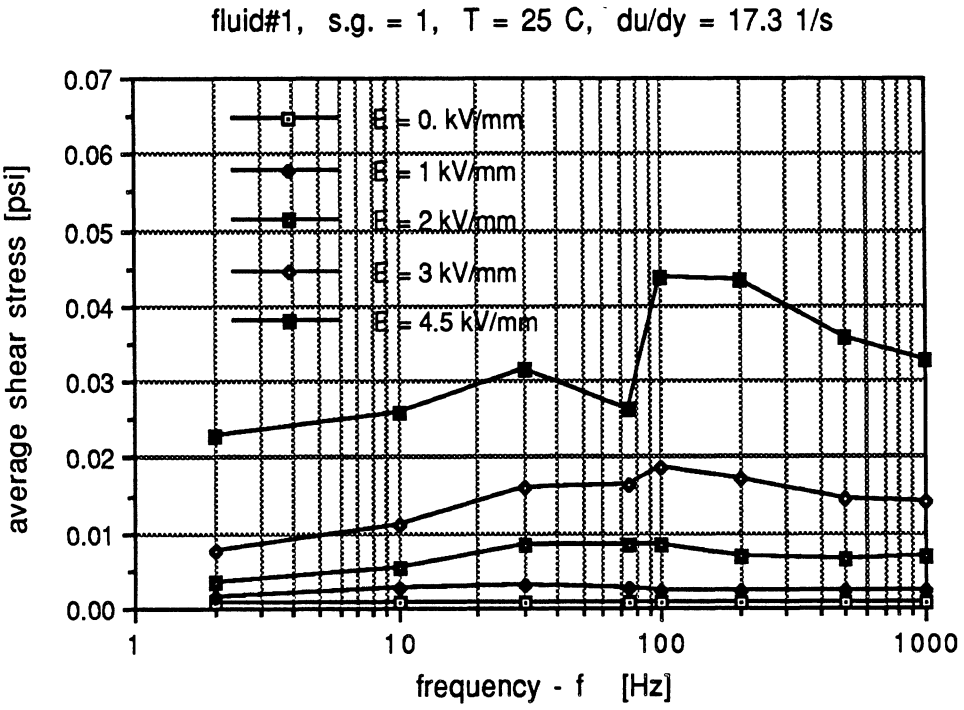


**Fig. 4.30. Frequency responses of average shear stress for fluid #1.**

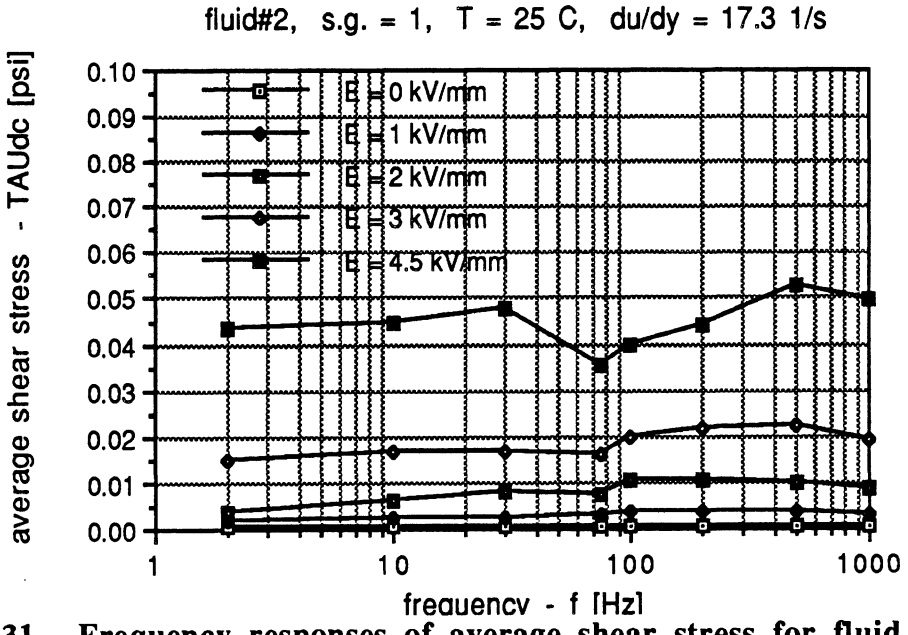


**Fig. 4.31. Frequency responses of average shear stress for fluid #2.**

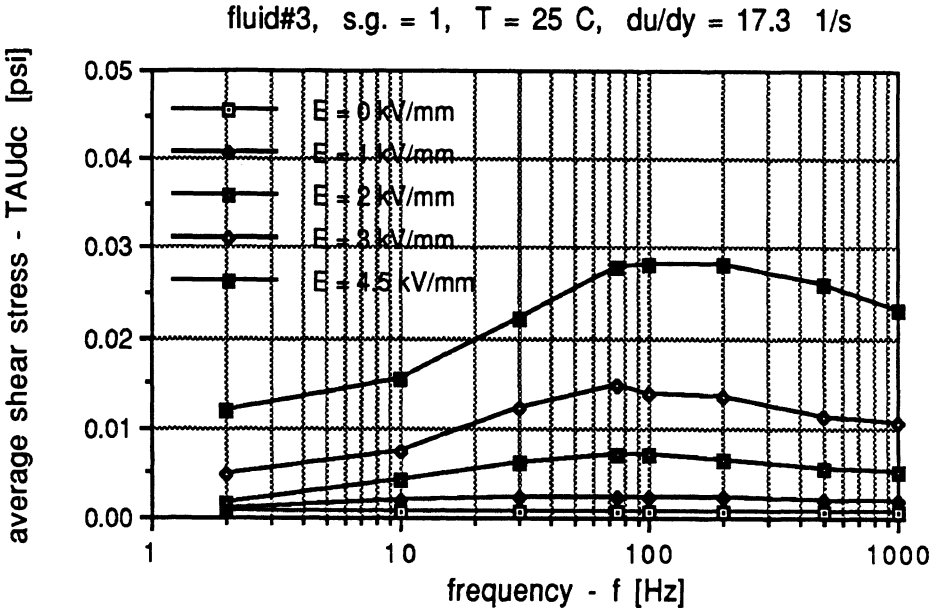


**Fig. 4.32. Frequency responses of average shear stress for fluid #3.**

Figs. 4.33, 4.34, and 4.35 show the variations of the peak, peak-to-peak, and time-average shear stresses at 4.5 kV/mm for fluids #1, #2, and #3, respectively. All three fluids show a significant resonance around 75 Hz, where the peak shear stress is several times higher than the low frequency value. This phenomenon was identified earlier as simply the result of the cup's rotational resonance on the torque transducer. The combination of attenuation in the peak-to-peak values above the resonance point and the sustained high-frequency value in the d.c. component, while suggesting that an ER response to the excitation sinusoid is still present, is simply clouded by the poor mechanical coupling which the transducer system affords.

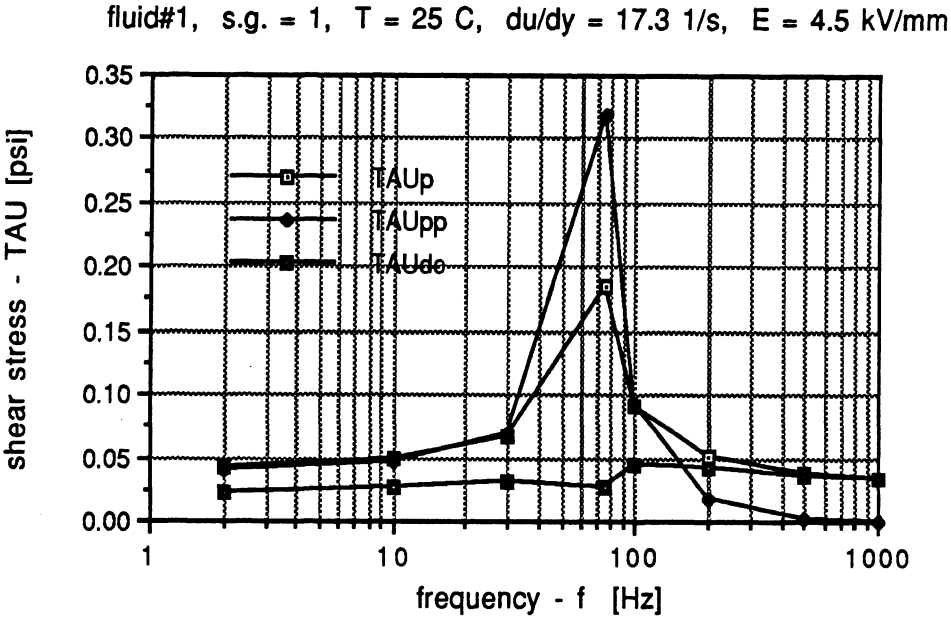


**Fig. 4.33. Frequency responses of the shear stress for fluid #1.**

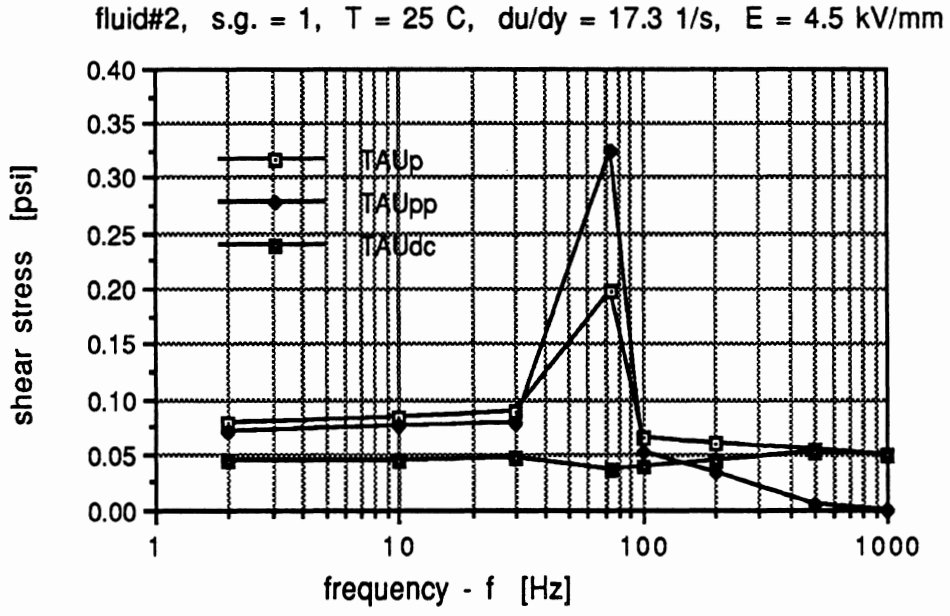


**Fig. 4.34. Frequency responses of the shear stress for fluid #2.**

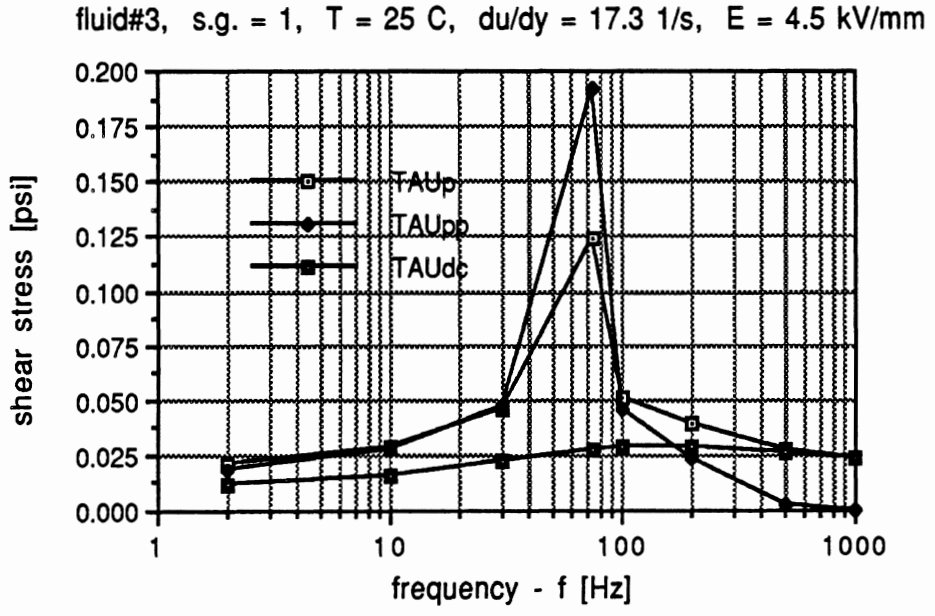


**Fig. 4.35. Frequency responses of the shear stress for fluid #3.**

Figs. 4.36, 4.37, and 4.38 show the current density for fluids #1, #2, and #3, respectively, over the broad frequency range. The current here represents the total output current $I_{out}$ from the amplifier. Therefore, at high frequencies the plotted variable is dominated by the capacitive current which is linearly related to the frequency, and the conductive current has become a minimal component. This contrast is illustrated in a specific case by the observation that the current density near zero frequency for fluid #2 is substantially higher than those for other two fluids. However, there is no substantial difference among the fluids at 1 kHz. It should also be noted that there is no noticeable variation in current density around the 75 Hz mechanical resonance point with all three fluids, suggesting that the high degree of mechanical activity due to cup oscillations in that region has no effect on the apparent conductance of the fluid.

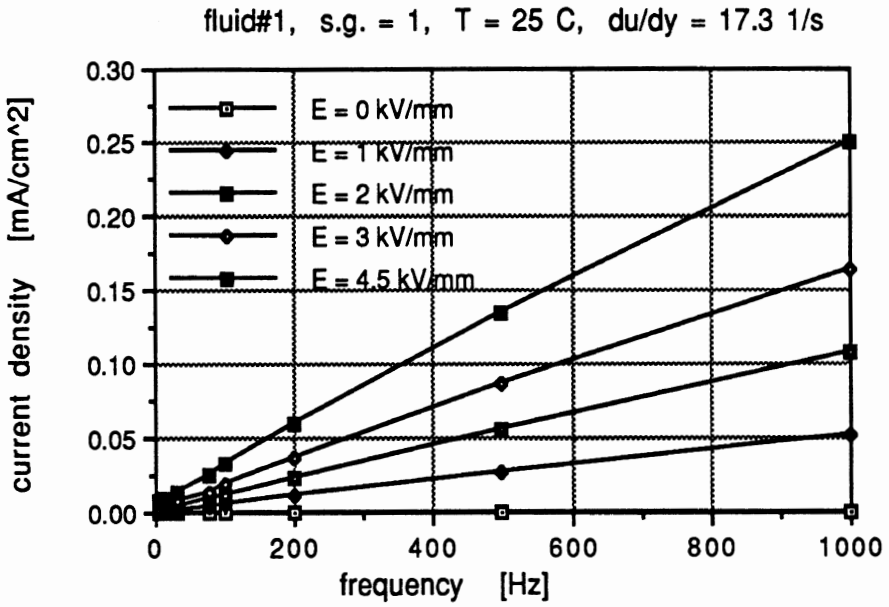


**Fig. 4.36. Frequency responses of the current density for fluid #1.**

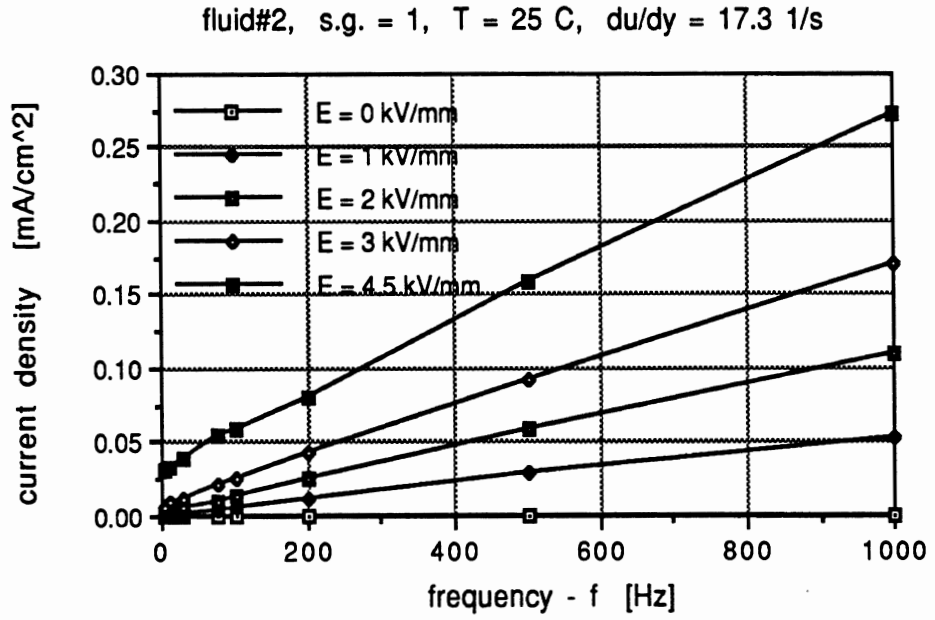


**Fig. 4.37. Frequency responses of the current density for fluid #2.**

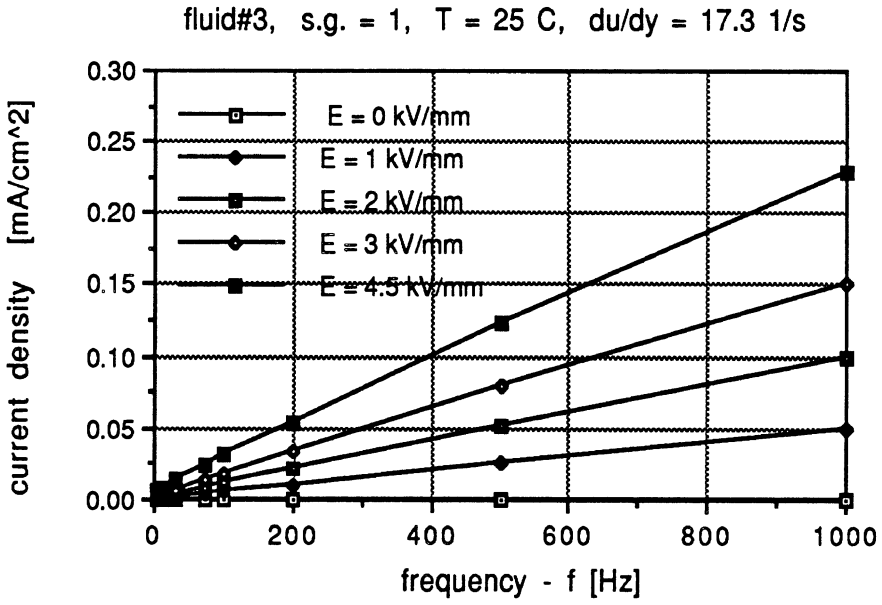


**Fig. 4.38. Frequency responses of the current density for fluid #3.**

## 4.12. Temperature Effect

The influence of temperature on the response of the ER fluids was measured as illustrated in Figs. 4.39 through 4.48. As expected of course, the results show the classical increase in current density with temperature, to such an extent that saturation of the amplifier's current capacity has a dominant effect on the appearance of the data at the higher temperature values. The amplifier used in this study provided a current limiting feature which yields saturation at 20 mA (r.m.s.). Given the area of the bob-cup assembly used in this study, the corresponding maximum current density is 0.40 mA/cm$^2$. Further, certain dynamic features of the saturation mechanism within the amplifier result in current limitations beginning at even lower levels (see, for example, the knee in the current density curve beginning at 0.30 mA/cm$^2$ in Fig. 4.40.)

Fig. 4.39 shows the plot of shear stress vs. temperature for fluid #1. We see a 75% increase in the shear stress as temperature increases from 25 to 30 degrees C, after which the shear stresses tend to be relatively stable until temperature reaches about 75 degrees C, at which point current saturation occurs as discussed above. Within the current saturation region the shear stresses drop dramatically.

As discussed in Section 4.9, the current density is strongly coupled with the shear stress. Thus, when an increasing temperature condition is imposed, after the amplifier has already reached saturation, the available current density is less than what is required to drive the ER mechanism, and shear stress level falls. Similar stress drops in the current saturation region are also observed for the other two fluids measured at selected excitation frequencies (see Figs. 4.41, 4.43, 4.45, and 4.47). For any fluid, of course, the saturation condition is reached at a higher value of temperature when the field strength (volts/mm) level is low. Indeed, when saturation occurs, and then the temperature level is further increased, the field strength begins to fall below the nominal target value.

The following discussion of shear stress variations will be limited to the data points corresponding to the region of non-saturated currents, which varies with the field strength. For fluid #2, the shear stresses show either flat or mildly increasing responses to temperature (Figs. 4.41, and 4.43). For fluid #3, the shear stresses at 10 Hz and 1000 Hz excitation, in Figs. 4.45 and 4.47, rise rather consistently over the temperature range until current saturation is reached.

Fluids #2 and #3 do not show the sharp increase in torque between 25 to 30 degrees C which appeared for fluid #1. Fluids #2 and #3 are still very effective at 125 degrees C, which is illustrated by their non-waning shear stress value at that temperature with E = 1 kV/mm. Unfortunately, no corresponding data were collected for fluid #1 at low-E values.

To further examine the effectiveness of the fluids at high temperature, tests are needed for lower values of the bob-cup projected area in order to avoid current saturation. In addition, temperatures above 120 degrees C produced a visible evaporation of the kerosene medium, thereby making tests at temperatures above 150 C impractical. Further, no measurements were made at temperatures below room ambient values for lack of refrigeration capability in these early experiments.

### *Discussion of the Temperature Effect Data*

In reflecting on the presented data showing the crucial temperature sensitivities, it is instructive to note other published findings and to consider an analytic characterization of the underlying mechanisms. Stevens et al. (1988) reported results showing the influence of temperature on both viscometer torques and current density for a fluid comprised of 350 cSt (at 23 degrees C) polydimethylsiloxane oil and starch mixed in equal ratio by mass. The current density data are similar to those produced here, although suffering saturation of the electrical power supply at the much lower level of 0.008 $mA/cm^2$. At high levels of field strength, viscometer torques consistently rise with temperature. At low field strength values, measured torques are relatively stable with temperature, showing only some mild peaks at 50-55 degrees C. Stevens attributed these peaks to the net result of two opposing effects, namely: (1) as the fluid temperature increases, the viscosity of the base fluid (and thus the viscous shear force) decreases, leading to an overall decrease in transmitted torque, and, (2) as temperature increases, the conductivity of the fluid and thus the current density increase, which produces an increase in the transmitted torque. In another study (Ushijima et al. 1988), viscosity slightly increases (less than 50%) as temperature changes from 20 to 70 degrees C, again suggesting that the two opposing mechanisms are more or less balancing one another.

Regardless of an individual fluid's variations in the specific gain of each effect, Stevens' explanation of the aggregate temperature effect is seen as reasonable, but perhaps incomplete. Close consideration of mechanisms (1) and (2), above, together with the recorded data, suggests a more complex total mechanism since the very strong rises in current density, driving shear stress levels up approximately linearly (see Sections 4.5 and 4.9), should produce a more strongly increasing torque response to temperature than is being measured.

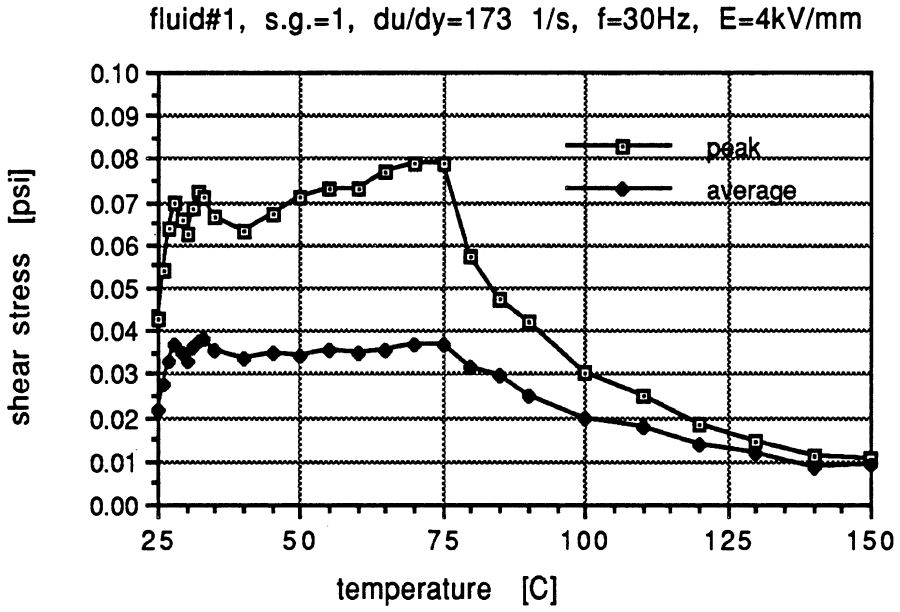


**Fig. 4.39 Temperature effect on the shear stresses for fluid #1.**

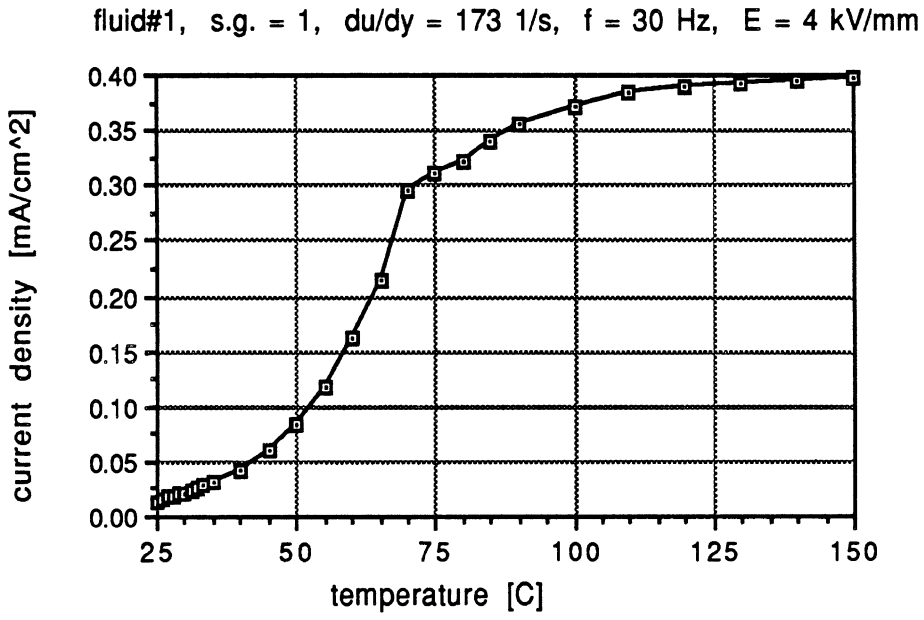


**Fig. 4.40 Temperature effect on the current density for fluid #1.**

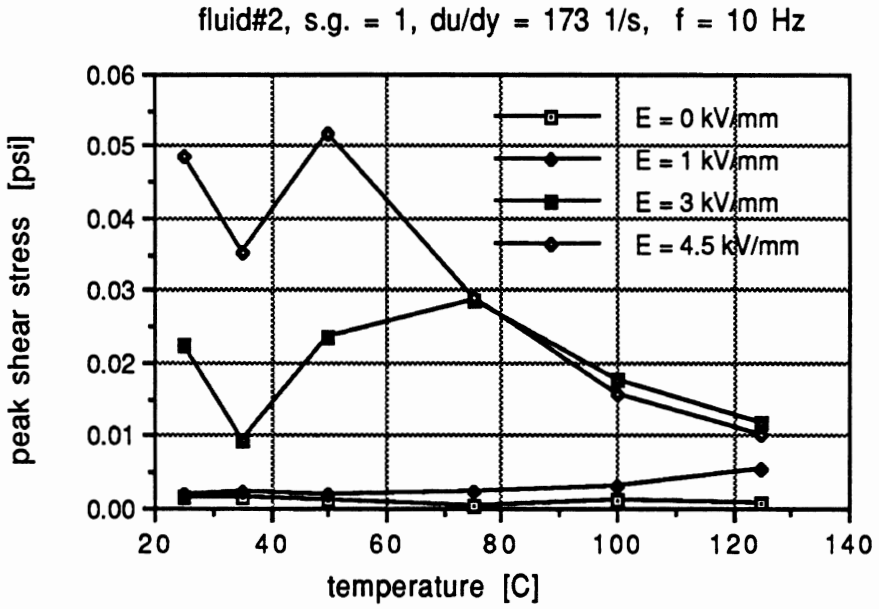


**Fig. 4.41 Temperature effect on the shear stresses at 10 Hz for fluid #2.**

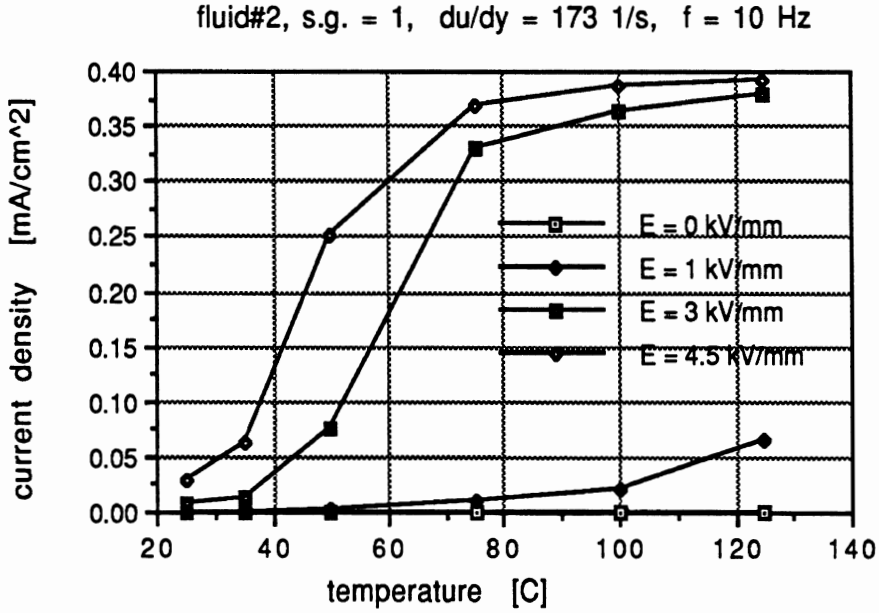


**Fig. 4.42 Temperature effect on the current density at 10 Hz for fluid #2.**

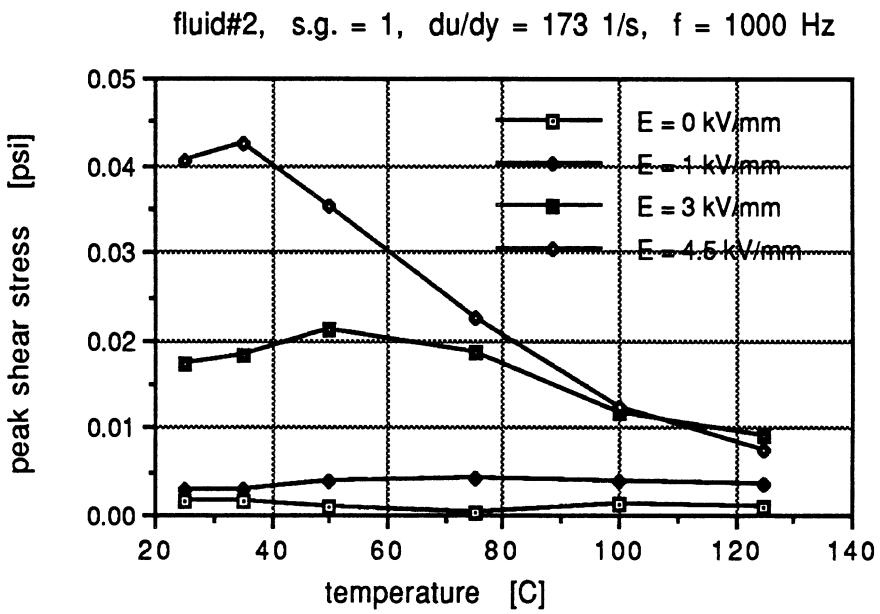


**Fig. 4.43 Temperature effect on the peak shear stress at 1 kHz for fluid #2.**

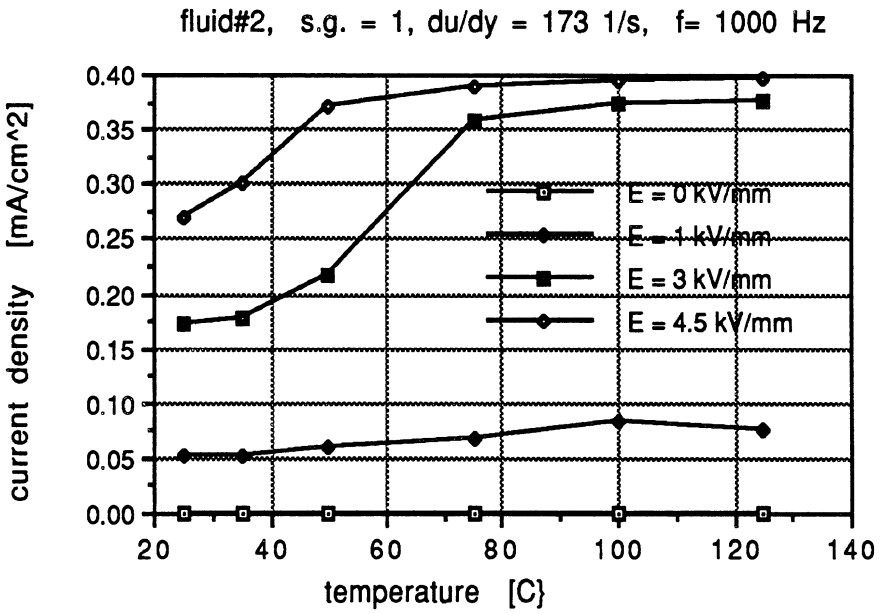


**Fig. 4.44 Temperature effect on the current density at 1 kHz for fluid #2.**

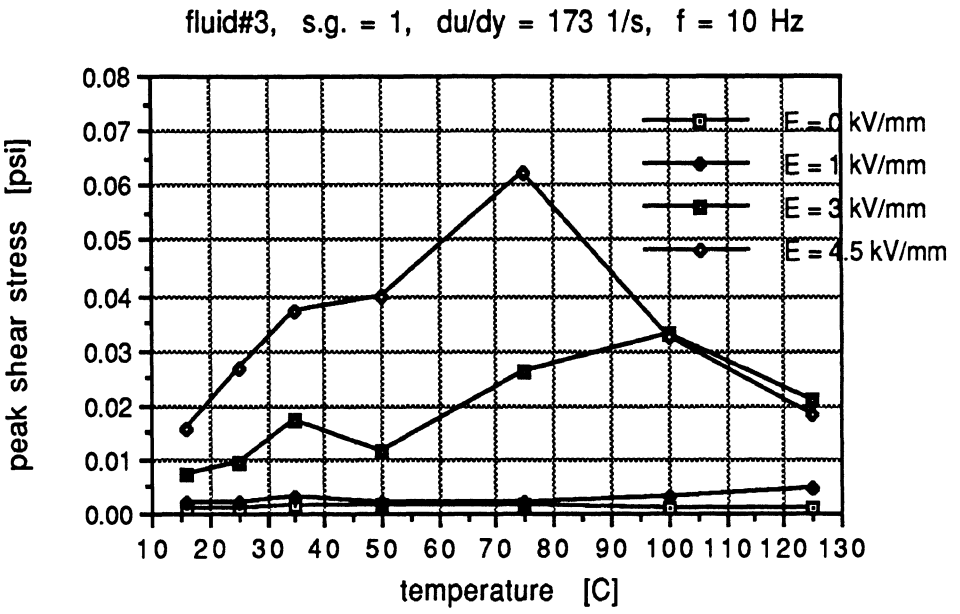


**Fig. 4.45 Temperature effect on the peak shear stress at 10 Hz for fluid #3.**

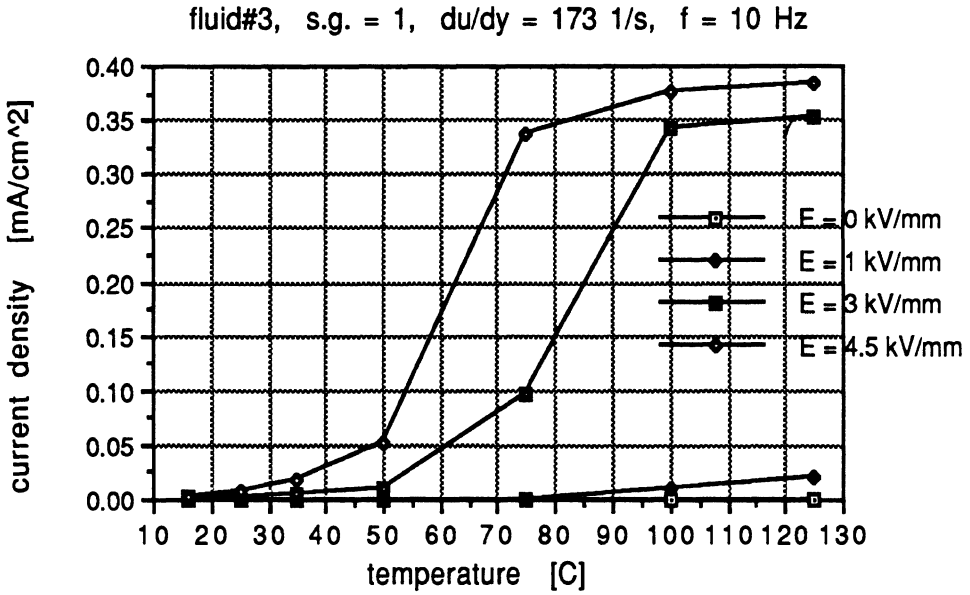


**Fig. 4.46 Temperature effect on the current density at 10 Hz for fluid #3.**

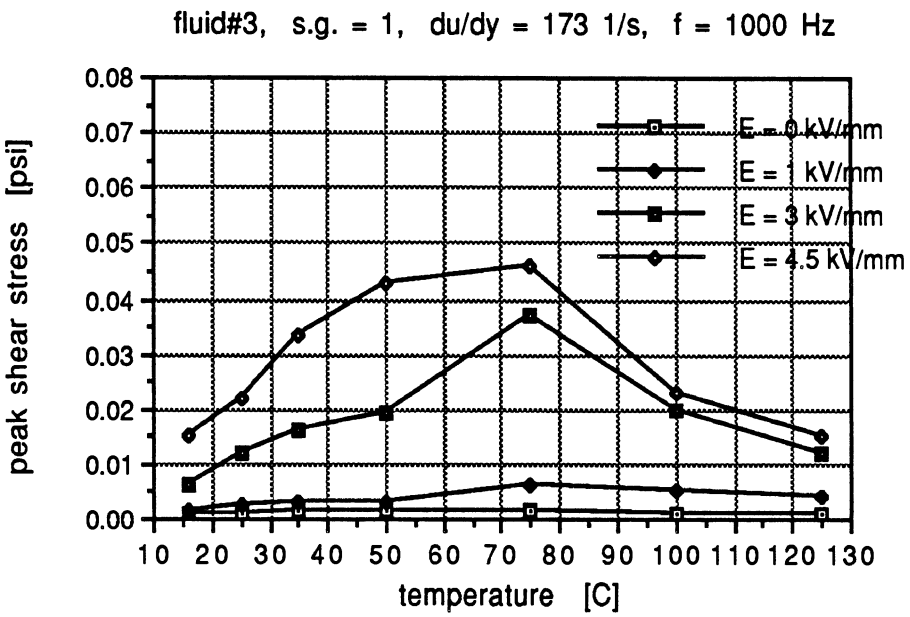


**Fig. 4.47 Temperature effect on the peak shear stress at 1 kHz for fluid #3.**

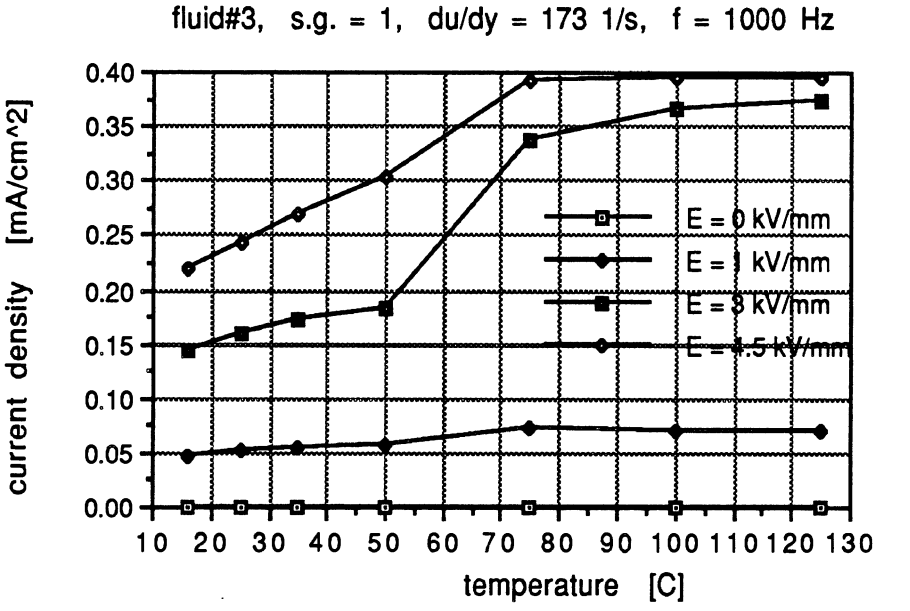


**Fig. 4.48 Temperature effect on the current density at 1 kHz for fluid #3.**

Fig. 4.49 shows an exponential curve fit to the data relating current density to temperature for fluid #3 at E = 4.5 kV/mm. The fitted function expresses the relationship:

$$CD = CD_0 2^{T/T_d}$$

where CD is the current density in $mA/cm^2$, $CD_0$ an intercept constant in $mA/cm^2$, T temperature in degrees C, and $T_d$ the temperature increment in degrees C over which CD doubles its value.

The data points at temperatures greater than 70 degrees C are not included in this illustration due to the current saturation. The exponential function provides a good correlation, as expected,

given the fundamental conductivity vs. temperature characteristic of the liquid phase (Filisko, 1989).

Quantitatively, the curve fitting equation in Fig. 4.49 can be re-written as:

$$CD = (.0011478)\ 2^{T/19.(}$$

which shows that the current density doubles for every 19 degrees C temperature increment. $CD_0$ and $T_d$ values for all the curves in Figs 4.40, 4.42, and 4.46 are listed in Table 4.3. For each case, the curve fit parameters apply to the non-saturated portions of the experimental range. The curve fitting has not been carried out for the data in Figs. 4.44 and 4.48 that apply to 1 kHz excitations for which the capacitive component of current dominates the total, and the conductive component is a minor contribution. Clearly, the current saturation condition is reached at much lower temperature values in Fig. 4.44 and 4.48 because of the high capacitive current load, even at the initial room temperature condition.

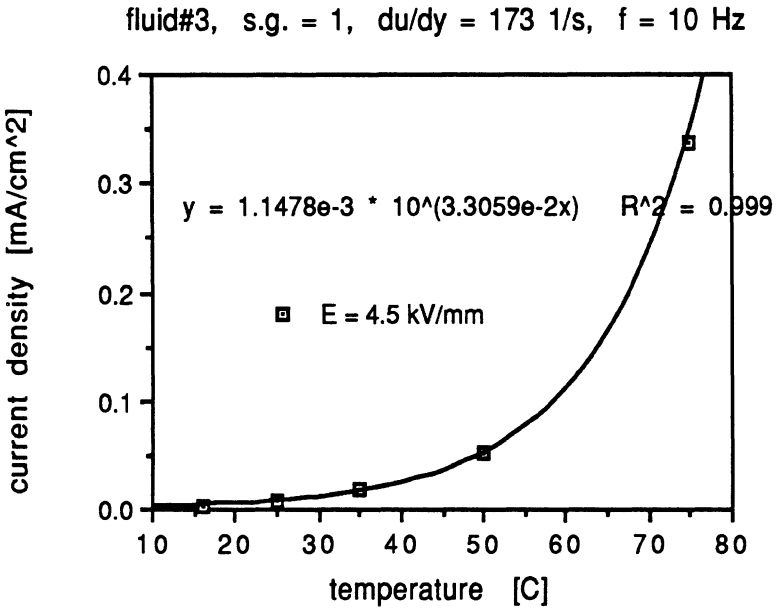


**Fig. 4.49. Curve fitting for the current density of fluid #3.**

**Table 4.3. Parameters for fitting the current/temperature relationship**

| fluid | Fig. | E. kV/mm | $CD_0$ mA/cm$^2$ | $T_d$ deg. C | correlation coefficient |
|---|---|---|---|---|---|
| #1 | 4.40 | 4.5 | .00292 | 10.4 | .997 |
| #2 | 4.42 | 1.0 | .00019 | 14.4 | .982 |
| #2 | 4.42 | 3.0 | .00111 | 8.93 | .980 |
| #2 | 4.42 | 4.5 | .00310 | 7.94 | .998 |

| | | | | | |
|---|---|---|---|---|---|
| #3 | 4.46 | 1.0 | .00018 | 19.0 | .873 |
| #3 | 4.46 | 3.0 | .00056 | 10.7 | .989 |
| #3 | 4.46 | 4.5 | .00115 | 9.1 | .999 |

The correlation coefficients in the right-hand column show that an exponential function represents the data extremely well, especially at high values of electric field strength. $T_d$ increases with electric field strength, indicating that the current density doubles its value more rapidly under stronger fields. Depending on the type of fluid and the voltage level, the current density doubles for a temperature increment between 7.94 and 19.0 degrees C.

This set of current density sensitivities can be compared with those reported by other investigators (Anon.; Stevens et al., 1988; Ushijima et al., 1988). Some investigator(s) (Anon.) reported that the current density approximately doubles every 6.6 degree C rise in temperature for some water-containing ER fluid. The data from Stevens et al. (1988) also indicate certain exponential behavior. However, the data from Ushijima et al. (1988) shows that the current density increase is more or less linear.

## 4.13. Settling Problems

The particulate phase in each of the sample fluids was observed to settle when left in a quiescent state. No quantitative study of the settling phenomenon was carried out here. In general, however, it was observed that the higher the solid content, the slower the settling rate and the less complete the segregation of phases over long periods of time. One favorable aspect of the settling observed with these water-free ER fluids is that, even after quiescent periods of a week or more, a homogenous mixture could be recovered after only mild mechanical disturbance or alternating electric excitation. In particular, these water-free fluids are immune from the strong hydrogen bonds which are seen as responsible for the "hard-settling" particulate phase in ER fluids which contain water. Nevertheless, the full practical significance of the particulate settling issue is yet to be explored.

## 4.14. Summary

The following summarizes the principal characteristics of the ER fluids tested in this study.

Under the zero-field condition, the formulated fluids behave as shear-thinning, non-Newtonian liquids even though the fluid base, kerosene, behaves as a Newtonian material.

An alternative component of the electric excitation is beneficial as a strategy preventing settling, causing particulate migrations and the formation of particulate clusters. Thus, even when the controlled system requires only low frequency, or nearly steady field control signals, the provision of high frequency signals as an agitation mechanism is useful.

In response to sinusoidal voltage excitation about zero potential, a viscometer's torque output wave form is (a) unipolar, (b) very close to sinusoidal, (c) at twice excitation frequency, and (d) offset above zero torque by slightly more than the amplitude of the torque sinusoid.

Negligible phase shift is observed in the current density and shear stress responses to imposed field strength at frequencies up to 1 kHz.

The natural frequency of the cup-torque sensor assembly in a viscometer is normally much less than the bandwidth of the ER fluids, which can lead to misinterpretation of the test data. Accordingly, some form of inverse data transformation is needed if one is to measure the broadband dynamic response of ER fluids using conventional viscometers.

The relationship between the Bingham stress and the electric field strength follows a power law. For example, fluid #2 in this study increased its Bingham stress limit according to the 2.5th power of the field strength.

Among three fluids tested, fluid #2 offers the highest Bingham stress, which is about 0.08 psi at moderate shear rate, an electric field strength of 4.5 kV/mm, and a solid content of 17.5%. A higher value can be achieved at a lower shear rate, a higher field strength, and a higher solid content.

The shear stress increases nonlinearly with the solid content. There is a solid content threshold, around 3 to 4% particulate in the mixture, above which the fluids formulated here begin to exhibit the ER effect.

The ratio of the energized fluid shear stress to the unenergized level is approaches two orders of magnitude, depending upon fluid formulation and field strength. The ratio was measured at 55, 97, and 44 for fluids #1, #2, and #3, respectively, (at E = 4.5 kV/mm, f = 10 Hz, s.g. = 1.0, du/dy = 17.3 1/s, and T = 25 degrees C.)

The conductive current through the ER fluids is the dominant component at low frequencies but recedes relative to the capacative component at frequencies approaching the bandwidth of the ER effect.

The Bingham stress is linearly dependent upon the conductive current density, at a constant temperature. Fluid #3 was seen to have the lowest current density values, amounting to approximately 0.018 $mA/cm^2$ at E = 4.5 kV/mm, du/dy = 17.3 1/s, s.g. = 1.0, excitation frequency = 10 Hz, and T = 25 degrees C, for a peak conductive power requirement of 0.1 $watts/cm^2$ .

The shear stress does not follow a perfect Bingham plastic model since the shear stress declines with shear rates, the largest drop coming at shear rate values of less than 100 mm/sec per mm.

The current density is relatively insensitive to shear rate.

The ER fluids formulated here show a strong shear stress response to field strength over a bandwidth of at least 1 kHz. From the relatively crude measurements possible here, a conservative estimate is that the shear stress response has fallen no more than 3 db over the first 1 kHz band—and may be considerably broader, yet, in bandwidth.

The total current density is almost linearly related to the excitation frequency at high frequencies due to the dominant contribution from the capacitive component of thecurrent.

The conductive current density is very sensitive to temperature. It doubles for every temperature increment of approximately 9 to 20 degrees C. The corresponding temperature increment value for current doubling decreases as the electric field strength increases.

The shear stress increases to a varying degree, depending on the type of fluid, as temperature increases. The zeolite-based fluids formulated here retain effectiveness at least up to the temperature level which was studied, 150 degree C.

In fluid #3, maleic anhydride was added to enhance shear stress level, with the expected side effect that current density would increase. However, the test data show shear stress levels to be lower and current density higher than those of two other fluid formulations studied.

# 5. ER VALVE AND BRIDGE ANALYSES

Before venturing into expensive and time-consuming processes of designing and fabricating ER valves and bridges, some theoretical analyses and simulations are needed to understand the nature and main parameters of their operations. Using the Bingham plastic fluid as the rheological model, the characteristics of a valve and a bridge are derived. Some basic parameter selection criteria for valve and bridge designs are recommended.

## 5.1. An ER Valve

The rheology of an ER fluid can be approximated as that of a Bingham plastic fluid (Section 4.3), which has the following constitutive equations:

$$\tau = \begin{cases} -\tau_y + \eta\dfrac{du}{dy} & \text{if } \dfrac{du}{dy} < 0 \\ \tau_y + \eta\dfrac{du}{dy} & \text{if } \dfrac{du}{dy} > 0 \end{cases} \tag{5.1}$$

or

$$\frac{du}{dy} = \begin{cases} \dfrac{\tau + \tau_y}{h} & \text{if } \tau < -\tau_y \\ 0 & \text{if } |\tau| \le \tau_y \\ \dfrac{\tau - \tau_y}{h} & \text{if } \tau > \tau_y \end{cases} \tag{5.2}$$

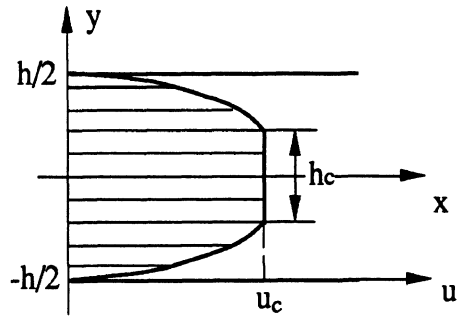


**Fig. 5.1. A flow between two parallel plates.**

For a two-dimensional fully-developed steady laminar flow between two parallel plates (Fig. 5.1), the governing equation is

$$\frac{dp}{dx} = \frac{d\tau}{dy} \tag{5.3}$$

which gives

$$\tau = \frac{dp}{dx} y \tag{5.4}$$

The shear stress changes linearly across the gap. Its value is equal to -/+ $\tau_y$ when y is at +/- $h_c/2$ (the edges of the blunt core of the flow), therefore

$$h_c = \frac{2\tau_y}{\frac{dp}{dx}} \tag{5.5}$$

where $h_c$ increases with $\tau_y$ and is inversely proportional to (-dp/dx). The maximum value $h_c$ can reach is h, when the pressure gradient (-dp/dx) is less than or equal to the following lock-up pressure gradient

$$(-\frac{dp}{dx})_c \equiv \frac{2\tau_y}{h} \tag{5.6}$$

or when the pressure drop $\Delta p$ is less than or equal to the following lock-up pressure drop, which is that value needed for overcoming the Bingham stress,

$$\Delta p_c \equiv 2(\frac{L}{h})\tau_y \tag{5.7}$$

where L is the length of the plates. The flow is completely stalled when $h_c$ is equal to h.

Substituting Eq. 5.2 into Eq. 5.4 and performing integration give the following velocity profiles:

$$u = \frac{1}{2\eta}(\frac{dp}{dx})[(\frac{h}{2})^2 - y^2] - \frac{\tau_y}{\eta}(\frac{h}{2} + y) \quad \text{when } -\frac{h}{2} \le y \le -\frac{h_c}{2} \tag{5.8a}$$

$$u = u_c = \frac{1}{8\eta(\frac{dp}{dx})}[h(\frac{dp}{dx}) - 2\tau_y]^2 \quad \text{when } |y| \le \frac{h_c}{2} \tag{5.8b}$$

$$u = \frac{1}{2\eta}(\frac{dp}{dx})[(\frac{h}{2})^2 - y^2] - \frac{\tau_y}{\eta}(\frac{h}{2} - y) \quad \text{when } \frac{h_c}{2} \le y \le \frac{h}{2} \tag{5.8c}$$

If the width of the plates is w, then the flow rate is

$$Q = \frac{w}{12\eta}(\frac{L}{\Delta p})^2[4\tau_y^3 - 3\tau_y h^2(\frac{\Delta p}{L})^2 + h^3(\frac{\Delta p}{L})^3] \tag{5.9}$$

When $\tau_y$ approaches zero, the flow rate becomes that of a Newtonian fluid

$$Q_N = \frac{h^3}{12\eta}\frac{w}{L}\Delta p \tag{5.10}$$

To simplify the analysis, the following two dimensionless parameters are defined

$$Q^* \equiv \frac{Q}{Q_N} \tag{5.11}$$

and

$$\Delta p^* \equiv \frac{\Delta p}{\Delta p_c} = \frac{\Delta p}{2(L/h)\tau_y} \tag{5.12}$$

where $\Delta p_c$ is the lock-up pressure drop as defined in Eq. 5.7. Q* is a dimensionless flow rate and $\Delta p^*$ is a dimensionless pressure drop. When $\Delta p^*$ is less than 1 or the pressure drop is less than the lock-up pressure drop, the flow rate Q or Q* will be zero. Substitution of Eqs. 5.10, 5.11 and 5.12 into Eq. 5.9 gives

$$Q^* = 1.0 - \frac{1.5}{\Delta p^*} + \frac{0.5}{\Delta p^{*3}} \qquad \text{if } \Delta p^* > 1 \tag{5.13a}$$

$$Q^* = 0 \qquad \text{if } \Delta p^* \le 1 \tag{5.13b}$$

The relationship between Q* and $\Delta p^*$ is also presented in Fig. 5.2. The maximum Q* value is 1.0; i.e., the maximum flow rate is equal to that of a Newtonian fluid, which can be achieved only by having an infinite pressure drop $\Delta p$ if the $\tau_y$ value is finite. In an ER valve, however, the region of interest is the one where a very small or zero Q* is delivered.

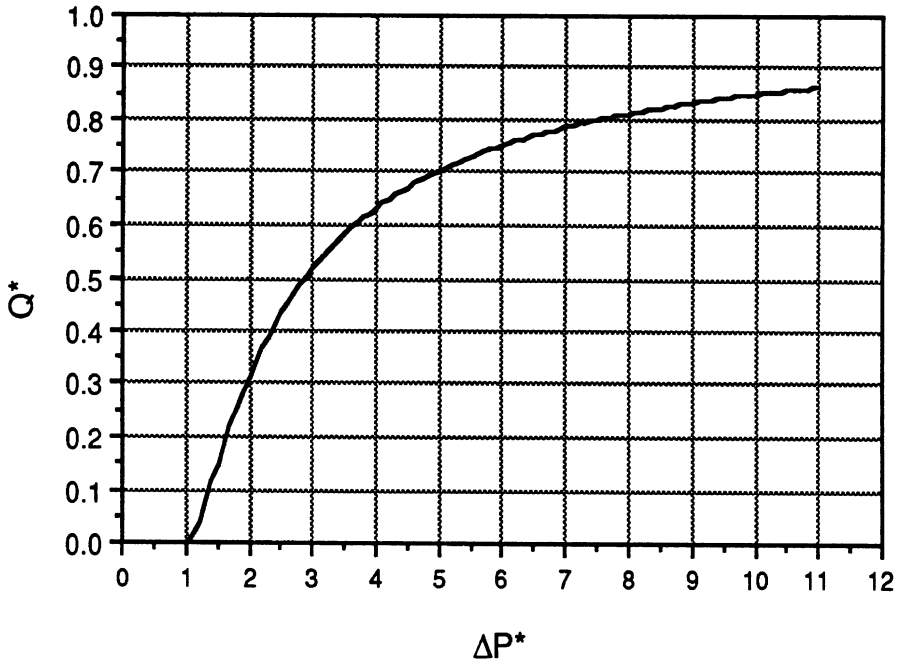


**Fig. 5.2. Flow characteristic of an ER valve.**

As shown in Eq. 5.13b and Fig. 5.2, Q* is 0 when $\Delta p^*$ is less than 1. If $\Delta p$ is 3,000 psi, h 1 mm, $\tau_y$ 1 psi, and $\Delta p^*$ is less than 1, then, according to Eq. 5.12, the valve length L has to be

equal to or longer than 1.5 meters. Such valves, which are able to completely stop flow against the full pressure head, may be practicably constructed from some form of labyrinth geometric designs which accumulate a long total shear length within a compact package.

## 5.2. An ER Bridge

An ER bridge, as illustrated in Fig. 5.3, consists of four ER valves which are arranged in analogy to the electrical Wheatstone bridge, to provide pressure amplification across a controlled load. That is, even if the valves installed in each arm are incapable of completely restraining the supply-level pressure drop, the full range of pressure control can be achieved across the diagonally-situated load, with resulting flow and power efficiencies to be defined by the analysis which is developed here. The load of the bridge can be either the "power spool" of a hydraulic valve or the hydraulic actuator itself. The flow directions and rates can be controlled by applying a combination of different electric fields to the four individual valves in the bridge.

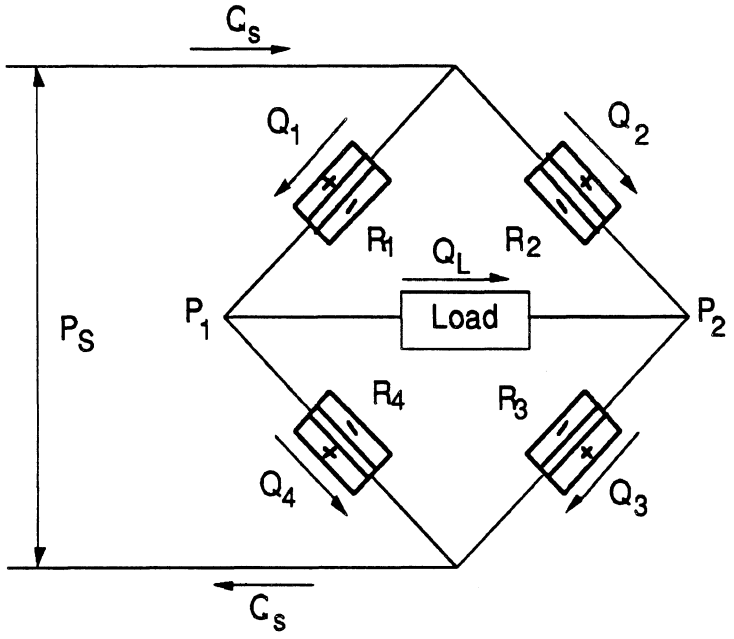


**Fig. 5.3. An ER bridge.**

The load pressure $P_L$ and load flow rate $Q_L$ are defined as follows:

$$P_L = P_1 - P_2 \tag{5.14}$$

$$Q_L = Q_1 - Q_4 \tag{5.15}$$

or

$$Q_L = Q_3 - Q_2 \tag{5.16}$$

where $P_1$ and $P_2$ are the exit pressures of ER valves 1 and 2, respectively. If $R_1$, $R_2$, $R_3$, and $R_4$ are the hydraulic resistances of the four ER valves, their flow rates can be calculated as follows:

$$Q_1 = \frac{P_s - P_1}{R_1} \tag{5.17}$$

$$Q_2 = \frac{P_s - P_2}{R_2} \tag{5.18}$$

$$Q_3 = \frac{P_2}{R_3} \tag{5.19}$$

$$Q_4 = \frac{P_1}{R_4} \tag{5.20}$$

The system flow rate $Q_s$ is calculated using the following equation:

$$Q_s = Q_1 + Q_2 = Q_3 + Q_4 \tag{5.21}$$

If the valves are designed and controlled in such a way that $R_3 = R_1$ and $R_4 = R_2$, then the following can be obtained:

$$P_s = P_1 + P_2 \tag{5.22}$$

$$P_1 = \frac{1}{2}(P_s + P_L) \tag{5.23}$$

$$P_2 = \frac{1}{2}(P_s - P_L) \tag{5.24}$$

$$Q_1 = Q_3 = \frac{\frac{1}{2}(P_s - P_L)}{R_1} \tag{5.25}$$

$$Q_2 = Q_4 = \frac{\frac{1}{2}(P_s + P_L)}{R_2} \tag{5.26}$$

$$Q_L = \frac{1}{2R_1R_2}[(R_2 - R_1)P_s - (R_2 + R_1)P_L] \tag{5.27}$$

$$Q_s = \frac{1}{2R_1R_2}[(R_2 + R_1)P_s - (R_2 - R_1)P_L] \tag{5.28}$$

The volumetric efficiency of the bridge is defined as

$$\eta_v \equiv \frac{Q_L}{Q_s} = \frac{(R_2 - R_1)P_s - (R_2 + R_1)P_L}{(R_2 + R_1)P_s - (R_2 - R_1)P_L} \tag{5.29}$$

The pressure efficiency of the bridge is defined as

$$\eta_P \equiv \frac{P_L}{P_s} \tag{5.30}$$

The power efficiency of the bridge is defined as

$$\eta_{power} \equiv \eta_v \eta_P \tag{5.31}$$

To simplify the analysis, the variables are normalized as follows

$$R^* \equiv \frac{R_2}{R_1} \tag{5.32}$$

$$P_L^* \equiv \frac{P_L}{P_s} = \eta_P \qquad (5.33)$$

$$Q_L^* \equiv \frac{Q_L}{Q_{L\,max}}$$

R* can be called relative flow resistance, the value of which is not only a function of electrical voltages applied to the valves but also an implicit function of flow conditions inside the valves, as analyzed later (Section 5.3). For a normal hydraulic system, $P_S$ is constant, and it is used as a reference pressure. $P_L$* is identical to $\eta_P$. $Q_S$ is not used as a reference flow rate because it is not a constant and changes with the load pressure and other system parameters. Instead, the maximum possible load flow rate, $Q_{L\,max}$ , is used and it is obtained when the system is load-free ($P_L = 0$) and two of the valves (valves 1 and 3 or 2 and 4) are completely closed.

If the analysis is limited to the working conditions where all the flow rates, the directions of which are shown in Fig. 5.3, are positive and the work is positive, i.e.,

$$P_L \geq 0$$

$$R_2 \geq R_1$$

$$Q_L \geq 0 \qquad (5.34)$$

then

$$Q_{L\,max} = \frac{P_s}{2R_1} \qquad (5.35)$$

and

$$Q_L^* = \frac{(R^*-1) - (R^*+1)P_L^*}{R^*} \qquad (5.36)$$

It appears that Eq. 5.36 gives the pressure-flow curve which is very important in bridge design. However, R* is also related to $P_L$*(see Section 5.3) in addition to other parameters, and it can not be treated as an independent variable. Rearranging Eq. 5.36 gives

$$P_L^* = \frac{(R^*-1) - R^*Q_L^*}{R^*+1} \qquad (5.37)$$

With the dimensionless variables defined above, the efficiencies can be expressed as:

$$\eta_v = \frac{(R^*-1) - (R^*+1)P_L^*}{(R^*+1) - (R^*-1)P_L^*} \qquad (5.38)$$

$$\eta_P = P_L^* \qquad (5.39)$$

$$\eta_{power} = \frac{(R^*-1)P_L^* - (R^*+1)P_L^{*2}}{(R^*+1) - (R^*-1)P_L^*} \qquad (5.40)$$

## 5.3. The Relative Flow Resistance R*

As shown in the previous section, the relative resistance R* is an important variable which is related to the calculations of the flow curve, volume efficiency and power efficiency. The objective of this section is to lay out the derivation of R*, itself.

As defined in Eq. 5.32, the relative flow resistance is

$$R^* = R_2 / R_1 \tag{5.41}$$

and

$$R_2 = \Delta P_2 / Q_2 \tag{5.42}$$

$$R_1 = \Delta P_1 / Q_1 \tag{5.43}$$

where $\Delta P_1$ is the pressure drop across valve 1, $\Delta P_2$ the pressure drop across valve 2. Substituting Eqs. 5.42 and 5.43 into Eq. 5.41 results in

$$R^* = \frac{\Delta P_2}{\Delta P_1}\frac{Q_1}{Q_2} \tag{5.44}$$

From Eq. 5.11,

$$\frac{Q_1}{Q_2} = \frac{Q_1^*}{Q_2^*}\frac{Q_{N1}}{Q_{N2}} \tag{5.45}$$

If the design of the bridge is symmetric, then, according to Eq. 5.10

$$\frac{Q_{N1}}{Q_{N2}} = \frac{\Delta P_1}{\Delta P_2} \tag{5.46}$$

and thus

$$\frac{Q_1}{Q_2} = \frac{Q_1^* \Delta P_1}{Q_2^* \Delta P_2} \tag{5.47}$$

Substituting the above equation into Eq. 5.44 gives

$$R^* = \frac{Q_1^*}{Q_2^*} \tag{5.48}$$

Using the reference case as assumed in the bridge analysis, namely that valves 2 and 4 are energized and valves 1 and 3 are not, then ,

$$Q_1^* = \frac{Q_1}{Q_{N1}} = 1 \tag{5.49}$$

$$Q^* \equiv Q_2^* = \frac{Q_2}{Q_{N2}} \neq 1 \tag{5.50}$$

$$R^* = \frac{1}{Q^*} \tag{5.51}$$

Substituting Eq. 5.13 into the above equation gives

$$R^* = \frac{\Delta P^{*3}}{\Delta P^{*3} - 1.5\Delta P^{*2} + 0.5} \qquad \text{if} \quad \Delta P^* > 1 \tag{5.52}$$

$$R^* = \infty \qquad \text{if} \quad \Delta P^* \le 1 \tag{5.53}$$

where

$$\Delta P^* = \Delta P_2^* = \frac{\Delta P_2}{\Delta P_c} = \frac{\Delta P_2}{2(L/h)\tau_y} \tag{5.54}$$

Because $\Delta P_2 = P_s - P_2 = P_s - (P_s - P_L)/2 = (P_s + P_L)/2$, therefore

$$\Delta P^* = \frac{\frac{1}{2}(P_s + P_L)}{\Delta P_c} \tag{5.55}$$

$\Delta P^*$ is a function of both the load pressure and the Bingham stress, as is $R^*$.

Let ,

$$\tau_y^* \equiv \frac{\Delta P_c}{P_s} = \frac{2(L/h)\tau_y}{P_s} \tag{5.56}$$

and

$$P_L^* \equiv \frac{P_L}{P_s} \tag{5.57}$$

then

$$\Delta P^* = \frac{1 + P_L^*}{2\tau_y^*} \tag{5.58}$$

The substitution of the above equation into Eqs. 5.52 and 5.53 gives

$$R^* = \frac{(1+P_L^*)^3}{(1+P_L^*)^3 - 3(1+P_L^*)^2\tau_y^* + 4\tau_y^{*3}} \qquad \text{if } P_L^* > 2\tau_y^* - 1 \tag{5.59a}$$

$$R^* = \infty \qquad \text{if } 0 \le P_L^* \le 2\tau_y^* - 1 \tag{5.59b}$$

Under the working condition assumed in this analysis, $P_L^*$ should be always greater than or equal to zero, therefore Eq. 5.59b will be useful only if $\tau_y^*$ is greater than 0.5. Eq. 59a is graphically presented in Fig. 5.4, from which it is clear that $R^*$ is a function of the load $P_L^*$ on the bridge as well as the level of the Bingham stress $\tau_y^*$. With a fixed value of $\tau_y^*$, the relative flow resistance and, thus, the ER effect decrease with an increasing $P_L^*$. Overall, the ER effect is

stronger with a higher Bingham stress $\tau_y^*$. When $\tau_y^*$ exceeds 0.5, there is a certain range of $P_L^*$, from 0 to $(2\tau_y^*-1)$, where R* is constant at infinite. That is, there is a saturation zone.

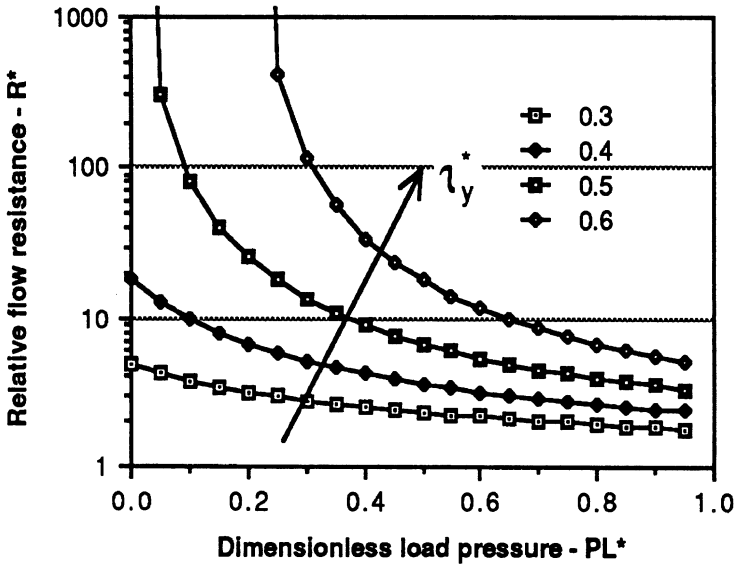


**Fig. 5.4. The dependence of R* on $P_L^*$ as well as $\tau_y^*$.**

## 5.4. ER Bridge Performance

As shown in Eqs. 5.36, 5.38, and 5.40, the flow rate, volumetric efficiency, and power efficiency are all functions of R* and $P_L^*$, while R* itself is a function of $P_L^*$ and $\tau_y^*$ (Eq. 5.59). If Eq. 5.59 is substituted into Eqs. 5.36, 5.38, and 5.40, the flow rate, the volume efficiency, and the power efficiency are all functions of $P_L^*$ and $\tau_y^*$ only, and are shown in Figs. 5.5 to 5.8. Therefore, R* served merely as an intermediate variable, and it can be eliminated in the calculation. $P_L^*$ and $\tau_y^*$ are two independent variables.

Looking at Fig. 5.5, which represents the case for which $\tau_y^*$ is 0.2, $Q_L^*$ is linearly related to $P_L^*$. $Q_L^*{}_{max}$ (the maximum value for $Q_L^*$), which is achieved when $P_L^* = 0$ (zero load pressure), is about 0.568 or 56.8% of $Q_{Lmax}$. The bridge is stalled at $P_L^* = P_L^*{}_{max} = 0.29$ where the load flow rate is zero. The load pressure $P_L^*$ can not go beyond $P_L^*{}_{max}$. The bridge can only use 29% of the available system pressure. The volume efficiency, $\eta_V$ (Evolume in Fig. 5.5,) follows the same pattern as $Q_L^*$. However, it is not linearly related to $P_L^*$. The power efficiency, $\eta_P$ (Epower in Fig. 5.5,) is equal to zero at both ends of the working range (from $P_L^* = 0$ to $P_L^* = P_L^*{}_{max}$), where either $Q_L^*$ or $P_L^*$ is equal to zero, which makes the product of $\eta_V$ and $P_L^*$ zero. The maximum power efficiency is reached in the middle of the working range, where the product of $\eta_V$ and $P_L^*$ reaches its maximum value. With $\tau_y^* = 0.2$, the maximum power efficiency is very small, about 0.58%. $P_L^*{}_{max}$, $Q_L^*{}_{max}$ , $\eta_{V\,max}$ and $\eta_{P\,max}$ increase with $\tau_y^*$.

For the case of $\tau_y^*$ equal 0.5 (Fig. 5.6) i.e. the lock-up pressure drop $\Delta P_C$ is half the system pressure the bridge can use up to 66% of the available system pressure. It can also use up to 100% of the available system flow rate, $Q_L^* = 1.0$, when, with no load pressure, a pair of valves in the bridged are just locked up by the ER effect. In order to achieve a pressure drop across the load, the bridge valves must be energized below the lock-up condition. The maximum power efficiency with $\tau_y^* = 0.5$ is about 24%.

As $\tau_y^*$ increases further, the working condition is much improved. If $\tau_y^* = 0.8$ (Fig. 5.7), $P_L^*{}_{max}$ can reach a value of .925; the maximum power efficiency is about 66%; and the bridge is able to lock up a pair of valves completely at a load pressure up to 60% of the system pressure. When $\tau_y^* = 1.0$ (Fig. 5.8), half of the bridge can be locked up during the entire working range, delivering up to 100% of the system pressure and 100% of the system flow rate to the load. The power efficiency is equal to $P_L^*$, which goes up to 100%.

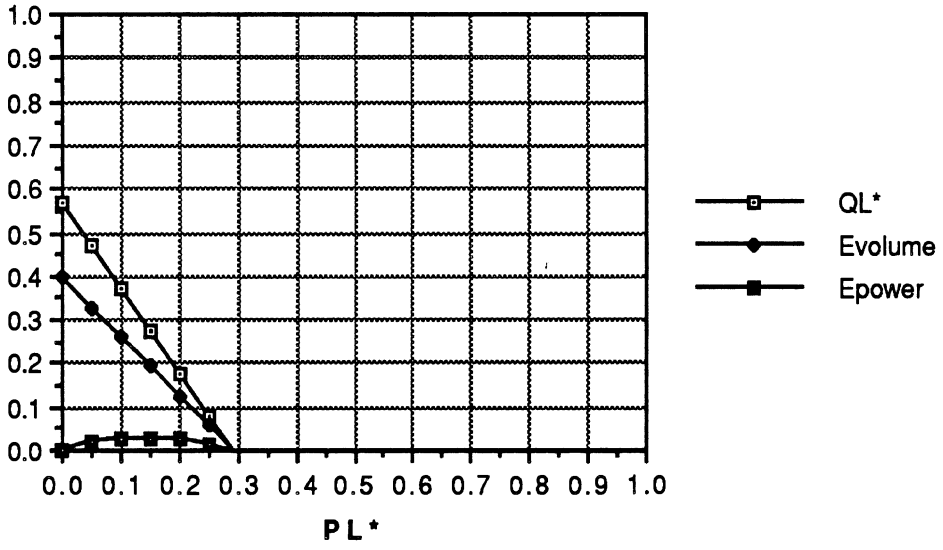


**Fig. 5.5. Bridge characteristics at $\tau_y^* = 0.2$.**

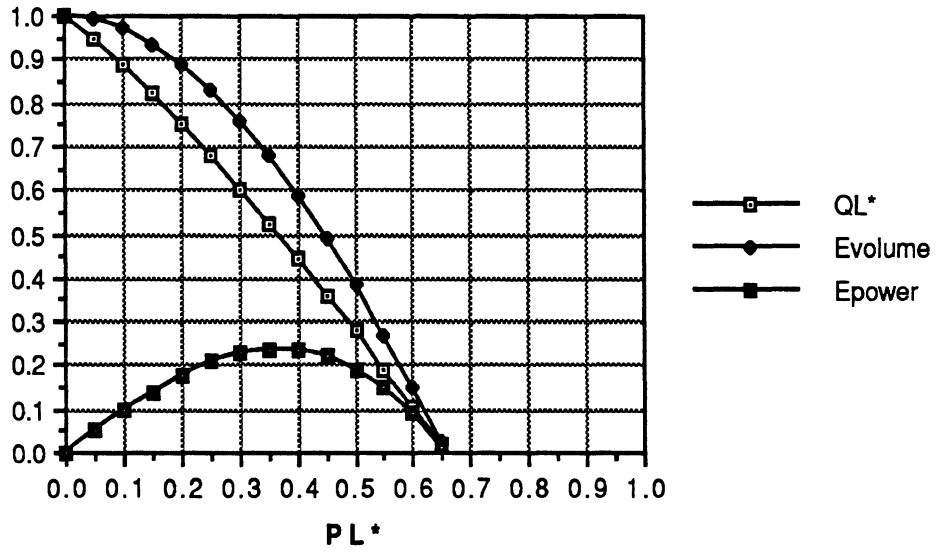


**Fig. 5.6. Bridge characteristics at $\tau_y^* = 0.5$.**

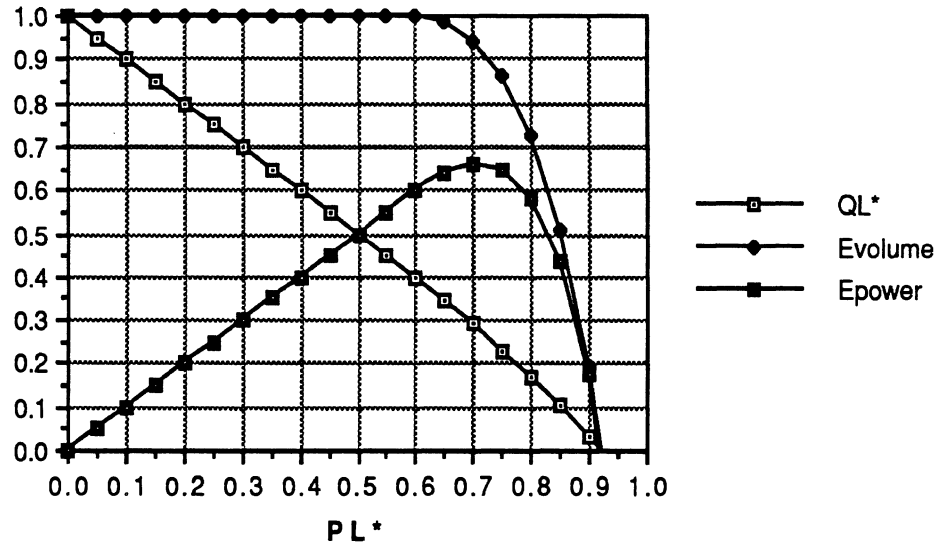


**Fig. 5.7. Bridge characteristics at $\tau_y^* = 0.8$.**

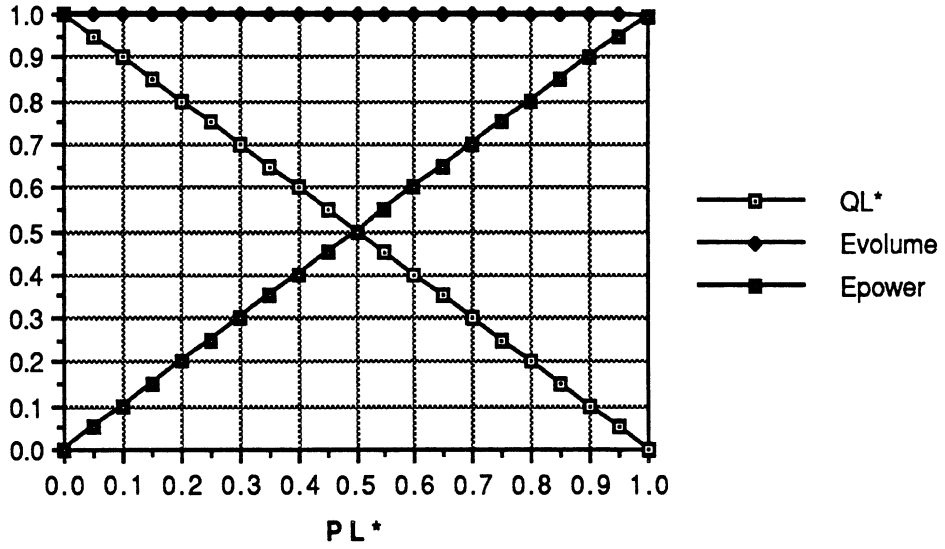


**Fig. 5.8. Bridge characteristics at $\tau_y^*$= 1.0.**

The maximum load flow rate and the maximum volumetric efficiency are obtained when the load pressure is zero. From Eqs. 5.36, 5.38 and 5.59

$$Q^*_{L\,max} = \begin{cases} 3\tau_y^* - 4\tau_y^{*\,3} & \text{if } \tau_y^* < 0.5 \\ 1 & \text{if } \tau_y^* \geq 0.5 \end{cases} \tag{5.60}$$

$$\eta_{v\,max} = \begin{cases} \dfrac{3\tau_y^* - 4\tau_y^{*\,3}}{2 - (3\tau_y^* - 4\tau_y^{*\,3})} & \text{if } \tau_y^* < 0.5 \\ 1 & \text{if } \tau_y^* \geq 0.5 \end{cases} \tag{5.61}$$

The maximum load pressure is obtained at zero load flow rate. From Eqs. 5.37 and 5.59

$$P^*_{L\,max} = \frac{3(1+P^*_{L\,max})^2\tau_y^* - 4\tau_y^{*3}}{2(1+P^*_{L\,max})^3 - 3(1+P^*_{L\,max})^2\tau_y^* + 4\tau_y^{*3}} \tag{5.62}$$

Since there is no closed-form solution for $P^*_{L\,max}$, an interative computation is required.

The maximum power efficiency is even more difficult to obtain analytically, and has not been attempted in this study. This value is simply illustrated in the numerical results which have been produced. The maximum volume efficiency, maximum load flow rate, maximum load pressure, and the maximum power efficiency are plotted with respect to the dimensionless Bingham stress in Fig. 5.9. All of them increase with the dimensionless Bingham stress. The higher the dimensionless Bingham stress of an ER bridge, the broader its working range will be and the more efficient the bridge will be.

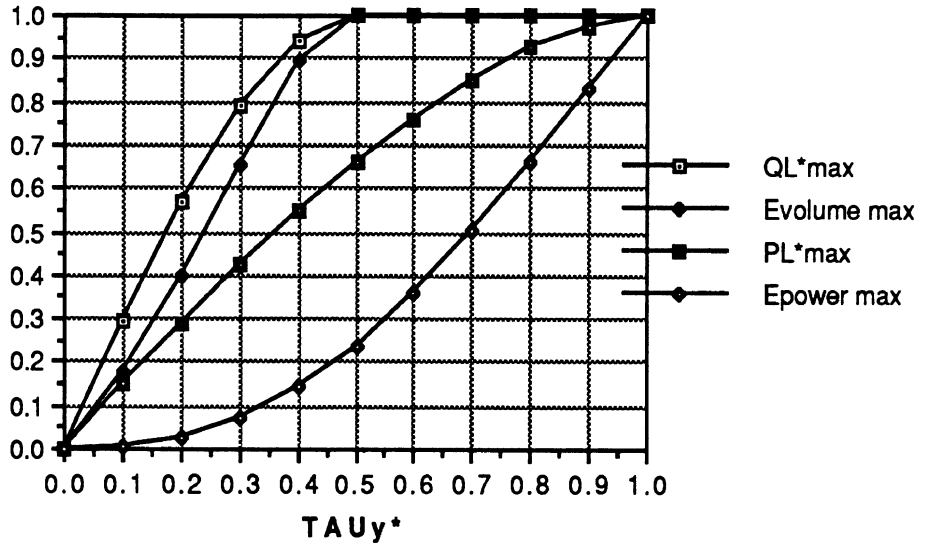


**Fig. 5.9 The effect of $\tau_y$*.**

From the above discussion, it is very clear that the value of $\tau_y$* has elementary importance for bridge design. Further, $\tau_y$* is not a constant for a given system. According to Eq. 5.56, it is a ratio of the lock-up pressure drop over the system pressure. For a given system pressure and a given geometric parameter, (L/h), $\tau_y$* linearly increases with $\tau_y$ which is mainly a nonlinear function of the electric field strength, E, in addition to many other parameters. In an automatic control system, the operating point of an ER bridge can be controlled by changing $\tau_y$*, which is directly regulated by adjusting the field strength.

## 5.5. ER bridge design

Eq. 56 can be re-written as

$$\frac{L}{h} = \frac{P_s}{2\tau_y} \tau_y^* \tag{5.63}$$

For a given fluid power system, $P_S$ is a given constant or system requirement. For a given ER fluid, $\tau_y$ is a variable; however it has an upper limit $\tau_{ymax}$. $\tau_y$* changes with $\tau_y$ for a given (L/h) and a given $P_S$, and it reaches the peak level, $\tau_y{}^*_{max}$, when $\tau_y$ is equal to $\tau_{ymax}$. Therefore,

$$\frac{L}{h} = \frac{P_s}{2\tau_{y\,max}} \tau_{y\,max}^* \tag{5.64}$$

which says that (L/h) depends on the selection of $\tau_y{}^*_{max}$. According to Fig. 5.9, the best choice is $\tau_y{}^*_{max}$ = 1.0, which gives the maximum values of flow rate, the load pressure, and the efficiencies. For example, if $\tau_{ymax}$ is 1 psi and $P_S$ is 3,000 psi, then (L/h) will be 1,500 with $\tau_y{}^*_{max}$ = 1.0. If the valve gap is 1.0 mm, then the total plate length for each valve should be 1.5

meters, which is indeed long but can be achieved in a compact package using labyrinth-plate valves (Section 3.2). When $\tau_y{}^*_{max} = 1.0$

$$2\frac{L}{h}\tau_{y\,max} = P_s \tag{5.65}$$

and according to Eq. 5.7,

$$\Delta p_{c\,max} = P_s \tag{5.66}$$

Therefore, the design criteria is fundamentally one of selecting (L/h) such that the maximum lock-up pressure drop is equal to the system pressure. If $\tau_{ymax}$ is too small, then L may become too long to be practicably fabricated. For example, if $\tau_{ymax}$ is 0.1 psi, then L must be 15 meters to keep $\tau_y{}^*_{max} = 1.0$. In another application of such a fluid, packaging constraints may require that, with $\tau_y{}^*_{max} = 0.1$, L is limited at 1.5 meters, thereby limiting the maximum load pressure to only 15% of the system pressure and the maximum power efficiency to only 0.58% according to Fig. 5.9.

As anticipated for the second phase of this study, if $\tau_{ymax}$ is 0.1 psi and L = 1.5 meter, the bridge will be able to deliver a maximum lock-up pressure of 300 psi, which will be sufficient for driving the main stage spool of a servo valve. With $\tau_y = 0.1$ psi and the valve geometries and system pressure selected such that $\tau_y{}^*_{max} = 1.0$, the bridge will be able to operate with up to 100% efficiency.

## 5.6. Summary

The main results from the analyses are:

The flow characteristic of a single ER valve has been derived with a Bingham plastic fluid model. For a constant electric field strength, the flow rate is nonlinearly related to the pressure drop. A no-flow zone exists in the low pressure region for a single ER valve, which is translated into a load flow-saturation zone at low load pressure for an ER bridge.

For an ER bridge, its volume and power efficiencies and the working range are related to the dimensionless load pressure and the dimensionless Bingham stress. The working range and efficiencies increase with the dimensionless Bingham stress. The efficiencies drop as the dimensionless load pressure rises.

With an ER fluid whose Bingham stress limit is 1 psi, and with ER valves whose internal shear length is 1.5 meters, a very efficient ER bridge can be built for a 3,000 psi fluid power system. With an ER fluid having a maximum Bingham stress of 0.1 psi , the same bridge would be able to deliver a 300 psi load pressure, which will be enough to drive the main stage spool of a servo valve.

# 6. CONCLUSIONS

A basic equipment ER devices laboratory has been assembled, with viscometer, valve-flow apparatus, and associated instrumentation and test methods developed. A continuous-flow ER fluid circuit has been designed for assembly during the follow-on study.

ER Valves of two configurations have been designed and fabricated. More sophisticated design concepts for ER valves and bridges are being studied.

The base data for three ER fluids have been collected, showing qualities of wide bandwidth (at least 1 kHz), high thermal stability (up to 125 or 150 degrees C), and moderate shear stress limits (close to 0.1 psi).

The performances of a single valve and a four-arm bridge using ER fluids have been analyzed, showing that a functional and efficient ER bridge is feasible.

The results suggest that it is feasible to build an ER bridge using the parallel-plate valve design concept and the fluids tested in the first phase of the study. With a Bingham stress of 0.1 psi and a valve length of 1.5 meters, an ER bridge will deliver up to 300 psi pressure drop, which will be sufficient to drive the main stage spool of a servo valve.

# REFERENCES


Anon. Electro-rheological fluids. Information Data Sheet. NBD-001-86-2507-4.5M 1086. American Cyanamid Company, Wayne, New Jersey, U.S.A. (a reference in Bullough and Peel 1988).

Brooks, D.A. (1982). Electro-rheological effect adds muscle. *Control & Instrument,* Vol.14, No.10, 57-59.

Bullough, W.A. (1988). Present trends and future research directions in electro-rheological fluids. *Proceedings of International Heat and Mass Transfer Forum,* Minsk, USSR, 24-27 May, 1988. To be published by the BSSR Academy of Sciences.

Bullough, W.A., and Peel, D.J. (1988). Progress towards a hydraulic semiconductor for vehicle application. *SAE Technical Paper Series* 881786, Passenger Car Meeting and Exposition, Dearborn, Michigan, Oct.31-Nov. 3.

Duclos, T.G., Acker, D.N., Carlson, J.D. (1988). Fluids that thicken electrically. *Machine Design,* Jan 21.

Filisko, F. (1989). Unpublished research results and communications, University of Michigan Department of Materials Science and Engineering. Ann Arbor, Michigan.

Gorodkin, R.G., Korobko, Ye.V., and Gleb, V.K. (1975). Rheology of polymer and disperse systems and rheophysics. Minsk, USSR.

Massey, I.C. (1971). Electroviscous effects in flow control systems. Unpublished report, Dept. of Mechanical Engineering, The University of Sheffield, 6 July.

Phillips, R.W. (1969). Engineering Applications of Fluids with a Variable Yield Stress. D. Eng. Dissertation, University of California, January .

Shoureshi, R., Graf, P.L., and Houston, T.L. (1986). Adaptive hydraulic engine mounts. *SAE Technical Paper Series* 860549. International Congress and Exposition, Detroit, Michigan, Feb. 24-28.

Shul'man, Z.P., Khusid, B.M., Korobkov, E.V., and Khizhinsky, E.P. (1987a). Damping of mechanical-system oscillations by a non-Newtonian fluid with electric-field dependent parameters. *Journal Non-Newtonian Fluid Mechanics,* 25:329-346.

Shul'man, Z.P, Khusid, B.M., Khizhinskii, B.P., Korobko, E.V. (1987b). Characteristics of an electrorheological damper in a vibration insulator. *Inzh.-Fiz. Zh.* (Byelorussian SSR) vol.52, no.2, pp.237-44.

Stangroom, J.E. (1983). Electro-rheological fluid. *Physics in Technology,* 14:290-296.

Stangroom, J.E., and Eckersley, J.S. (1985). Pipework snubbers based on electro-rheological fluids. In: *Pipework Design and Operation Conf.*, (London, U.K.: Feb. 19-20, 1985). Bury St. Edmunds, U.K., Mech. Engng. Publications Ltd., Paper C29/85, p.279-284. (IMechE Conference Publications 1985-1).

Stanway, R., Sproston, J.L, and Stevens, N.G. (1985). Non-linear identification of an electro-rheological vibration damper. *Proceedings 7th IFAC Symposium on Identification and System Parameter Estimation,* York, U.K., pp.195-200.

Stanway, R., Sproston, J., Firoozian, R. (1989a). Identification of the damping law of an electro-rheological fluid: A sequential filtering approach. *Journal of Dynamic Systems, Measurement and Control,* Vol.111, no.1, pp.91-96.

Stanway, R., Sproston, J.L., and Wu, X. (1989b). Variable suspension damping using electro-rheological fluids. IMechE, C382/034, pp.547-558.

Stevens, N.G., Sproston, J.L., and Stanway, R. (1984). Experimental evaluation of a simple electroviscous damper. *Journal of Electrostatics*, 15:275-283.

Stevens, N.G., Sproston, J.L., and Stanway, R. (1988). An experimental study of electro-rheological torque transmission. *Journal of Mechanisms, Transmissions, and Automation in Design*, vol.110, no.2, pp.182-188.

Uejima, H. (1972). *Japan Journal of Applied Physics*, vol.11, no.3, p.319.

Ushijima, T., Takano, K., Noguchi, T. (1988). Rheological characteristics of ER fluids and their application to anti-vibration devices with control mechanism for automobiles. *SAE Technical Paper Series 881787.* Passenger Car Meeting and Exposition, Dearborn, Michigan, Oct. 31 - Nov.3.